Mountain permafrost in the Central Pyrenees: insights from the Devaux ice cave

Miguel Bartolomé[1*], Gérard Cazenave[2], Marc Luetscher[3], Christoph Spötl[4], Fernando Gázquez[5,6], Ánchel Belmonte[7], Alexandra V. Turchyn[8], Juan Ignacio López-Moreno[1], Ana Moreno[1]

1 Departamento de Procesos Geoambientales y Cambio Global, Instituto Pirenaico de Ecología-CSIC, Zaragoza, Spain.

2 Société de Spéléologie et de Préhistoire des Pyrénées Occidentales (SSPPO),5 allée du Grand Tour, 64000 PAU, France

3 Swiss Institute for Speleology and Karst Studies (SISKA), La Chaux-de-Fonds, Switzerland

4 Institute of Geology, University of Innsbruck, 6020 Innsbruck, Austria

5 Water Resources and Environmental Geology Research Group, Department of Biology and Geology, University of Almería, Almería, Spain.

6 Andalusian Centre for the Monitoring and Assessment of Global Change (CAESCG), University of Almería, Almería, Spain.

7 Sobrarbe-Pirineos UNESCO Global Geopark. Boltaña. Spain.

8 Godwin Laboratory for Palaeoclimate Research, Department of Earth Sciences, University of Cambridge, Cambridge, UK

*Correspondence: Miguel Bartolomé (mbart@ipe.csic.es)

Abstract (250words)

Ice caves are one of the least studied parts of the cryosphere, particularly those located in inaccessible permafrost areas at high altitudes or high latitudes. We characterize the climate dynamics and the geomorphological features of Devaux cave, an outstanding ice cave in the Central Pyrenees on the French-Spanish border. Two distinct cave sectors were identified based on air temperature and

geomorphological observations. The first one comprises well-ventilated galleries with large temperature oscillations likely influenced by a cave river. The second sector corresponds to more isolated chambers, where air and rock temperatures stay below 0ºC throughout the year. Seasonal layered ice and hoarfrost occupy the first sector, while transparent, massive perennial ice is present in the isolated chambers. Cryogenic calcite and gypsum are mainly present within the perennial ice. During winter, the cave river freezes at the outlet, resulting in a damming and back-flooding of the cave. We suggest that relict ice formations record past damming events with subsequent formation of congelation ice. $\delta^{34}S$ values of gypsum indicate that the sulfate originated from the oxidation of pyrite present in the bedrock. Several features including ~~the~~ air and rock temperatures, the absence of drips, the ~~low~~ small loss of ice in the past seven decades, and the location of ice bodies in the cave indicate that the cave permafrost is the result of a combination of undercooling by ventilation and diffusive heat transfer from the surrounding permafrost, reaching a thickness of ~200 m ~~below the surface~~.

Keywords: Ice cave, cave monitoring, cryogenic cave carbonates, cryogenic gypsum, ~~Devaux cave~~Pyrenees.

1. Introduction

Mountain areas are ~~one of the most susceptible~~among those environments ~~to~~ most affected by current climate change (Hock et al., 2019). In the mid-latitudes, high-altitude areas are subject to mountain permafrost, a very sensitive and unstable phenomenon that responds quickly to environmental changes (Harris et al., 2003; Biskaborn et al., 2019) due to the number of factors. ~~They influence the spatial distribution of mountain permafrost, including snow cover distribution and thickness, topography, water availability, surface temperature and rock temperature~~Snow cover distribution and thickness, topography, water availability, and surface and rock temperature influence the spatial distribution of mountain permafrost (Gruber and Haeberli, 2009). In light of these processes, ~~Due to this number of processes~~ multidisciplinary studies including, among others, measurements of rock temperature ~~measurements~~ in boreholes~~,~~ and ~~the~~ bottom temperatures of snow cover (BTS), ~~a variety of~~ geophysical techniques, and ~~thematic~~ detailed ~~maps~~ mapping (geomorphology, thermal) are needed to gain a

Comentado [M1]: Reviewer #2.
l55-57: (R) snow cover distribution and thickness, topography, water availability, surface and rock temperature all influence the spatial distribution of mountain permafrost

Comentado [M2]: Reviewer #2.
l57-61: (R) In light of these processes, [...] are needed to gain a comprehensive understanding of mountain permafrost.

comprehensive understanding of mountain permafrost (e.g. Lewkowicz and Ednie, 2004; Serrano et al., 2019; Biskaborn et al., 2019). On the other hand, ~~the~~ integrated ~~study~~ studies of paleo-permafrost (~~e.g. Vaks et al., 2020),~~ e.g. Vaks et al., 2020) and modern permafrost, specifically mountain permafrost (e.g., Supper et al., 2014; Scandroglio et al., 2021), sheds~~s~~ light on past, present and future developments of permafrost areas, an issue of vital importance in the context of global warming. Studies of past permafrost require sedimentary records, which are locally preserved in caves located at high altitudes and/or high latitudes. ~~Thus, t~~Temporal and spatial changes in past permafrost distribution have been identified using speleothems (stalagmites, flowstones) in high-latitude~~circumpolar~~ and polar regions (e.g., (Vaks et al., 2013, 2020; Moseley et al., 2021; Li et al., 2021) as well as in mid-latitude regions (e.g., Lundberg and McFarlane, 2007; Fankhauser et al., 2016; Lechleitner et al., 2020).

Ice caves are ~~defined as~~ cavities in rock hosting perennial ice that results from the transformation of snow and/or the freezing of infiltrating water ~~reaching the cave~~ (Perşoiu and Lauritzen, 2018). Cave ice can be dated and used as a valuable paleoclimate archive in non-polar areas (e.g., Stoffel et al., 2009; Spötl et al., 2013; Perșoiu et al., 2017; Kern et al., 2018; Sancho et al., 2018a; Leunda et al., 2019; Munroe, 2021; Racine et al., 2022). ~~Furthermore, temporal and spatial changes in past permafrost distribution have been identified using speleothems (stalagmites, flowstones) in circumpolar and polar regions (e.g., as well as in mid-latitude regions (e.g., Lundberg and McFarlane, 2007; Fankhauser et al., 2016; Lechleitner et al., 2020).~~ Recently, coarse cryogenic cave carbonates (CCC_{coarse}), that form during slow freezing of water inside caves, have been used as indicator of permafrost degradation, permafrost thickness, and subsurface ice formation (Žák et al., 2004, 2012; Richter et al., 2010a; Luetscher et al., 2013; Orvošová et al., 2014; Spötl and Cheng, 2014; Bartolomé et al., 2015; Dublyansky et al., 2018; Koltai et al., 2020; Munroe et al., 2021; Spötl et al., 2021).

Many ice caves are located in areas where the mean annual air temperature (MAAT) outside the cave is above 0ºC (Perşoiu and Lauritzen, 2018) and, therefore, are highly susceptible to future climate warming (Kern and Perşoiu, 2013). These ice caves are local thermal anomalies which are controlled by the

Comentado [M3]: New reference added:

Li, T.-Y., Baker, J. L., Wang, T., Zhang, J., Wu, Y., Li, H.-C., Blyakharchuk, T., Yu, T.-L., Shen, C.-C., Cheng, H., Kong, X.-G., Xie, W.-L., and Edwards, R. L.: Early Holocene permafrost retreat in West Siberia amplified by reorganization of westerly wind systems, Commun. Earth Environ., 2, 1–11, https://doi.org/10.1038/s43247-021-00238-z, 2021.

Comentado [M4]: Reviewer#1: lines 73-78: This sentence somehow doesn't fit to the other parts of this paragraph. Please consider omitting it or moving it to another place where it fits better.

Con formato: Inglés (Estados Unidos)

Comentado [M5]: added:
Racine, T. M. F., Reimer, P. J., and Spötl, C.: Multi-centennial mass balance of perennial ice deposits in Alpine caves mirrors the evolution of glaciers during the Late Holocene, Sci. Rep., 12, 11374, https://doi.org/10.1038/s41598-022-15516-9, 2022.

Con formato: Inglés (Estados Unidos)

Código de campo cambiado

Comentado [M6]: Moved from here to lines 70-75

Comentado [M7]: New reference added:

Spötl, C., Koltai, G., Jarosch, A. H., and Cheng, H.: Increased autumn and winter precipitation during the Last Glacial Maximum in the European Alps, Nat. Commun., 12, 1839, https://doi.org/10.1038/s41467-021-22090-7, 2021.

cave geometry and the associated ventilation pattern. Their ice deposits represent sporadic permafrost occurrences and do not inform about the wider thermal environment. In contrast, at high altitudes and high latitudes subsurface ice deposits are still preserved by the presence of permafrost under the current climate ~~change~~ conditions. There, mountain permafrost is limited to areas where a periglacial belt is present, with MAAT ≤ 0º C. For example, in the European Alps, discontinuous mountain permafrost is observed ~~between~~ above 2600 ~~and~~ to 3000 m a.s.l. (Boeckli et al., 2012), while in southern Europe permafrost is generally absent (i.e. not observed even on the highest massif of the Iberian Peninsula, Gómez-Ortiz et al., 2019). In the Central Pyrenees few studies suggest the possible presence of permafrost above 2750 m a.s.l. (Serrano et al., 2019, 2020; Rico et al., 2021), and the presence of a few ice caves has only recently been documented (e.g. Sancho et al., 2018a; Serrano et al., 2018) informing about the occurrence of sporadic permafrost. ~~.~~

The aim of this study is to characterize the permafrost conditions in Devaux cave, a high-altitude ice cave in the Central Pyrenees. We monitored air, water and rock temperatures and used cryogenic cave deposits to i) document the distribution of permafrost within this cave, and ii) to study the processes that resulted in perennial cave ice bodies and associated cryogenic mineral occurrences.

2. Study site

Devaux cave opens at ~2838 m a.s.l. in the NE cliff of Gavarnie cirque (France) of the Monte Perdido massif (MPm) in the Central Pyrenees (Fig. 1a). The cave is located between the Parc National des Pyrénées (France) and the Parque Nacional de Ordesa y Monte Perdido (Spain). Named after Joseph Devaux who discovered and explored it in 1928, the cave was later investigated with respect to its hydrogeology and microclimatology and preliminary descriptions of its deposits were reported (e.g., Devaux, 1929; 1933; Rösch and Rösch, 1935; Rösch, 1949; d~~D~~u Cailar and Dubois, 1953; Requirand, 2014).

Comentado [M8]: Reviewer #2
A)l90-91:
In contrast, at high altitudes and high latitudes ice deposits are still preserved under the current climate change may be in relation to the permafrost presence.

Done

Comentado [M9]: Reviewer #2
l98-99: (T) the presence of a few ice caves has only recently been documented

Done

Comentado [M10]: Reviewer #2
B) l98-99:

), informing about sporadic permafrost

Done

The area is dominated by limestones and dolostones ranging from the Upper Cretaceous to the Eocene-Paleocene. MPm is the highest limestone karst area in Europe reaching up to 3355 m a.s.l. (Monte Perdido peak) (Fig. 1b). The nearest peaks to Devaux cave are Marboré (3248 m a.s.l.) and the three Cascada peaks (3164 m, 3111 m, and 3098 m a.s.l.). The limestone thickness above the cave varies between ~200 and 250 m (Fig. 2a). In Devaux, the galleries follow the axis of a NW-SE striking syncline (Fig. 1b). A river runs along the cave (Fig. 2a, b). The cave has two known entrances: the lower one corresponds to the main outlet of the cave river (Brulle spring, North 1, ~2821 m a.s.l.), while the upper entrance is known as the "Porche" (South, ~2836 m a.s.l.) (Figs. 1c and 2b). Between these two entrances, a small gallery (Spring North 2) opens +1.2 m above Brulle spring (Fig. 1c). Brulle is one of the main springs in the Gavarnie cirque. This spring drains a catchment of ~2.6 km^2 (polje) located on the southern face of MPm between ~2850 and 3355 m a.s.l. (Figs. 1b and, 1d). Major water flow is observed during late spring and early summer when snowmelt ~~recharges~~ occurs in a catchment characterised by shafts, sinkholes and small closed depressions (Fig. 1d). The water of Brulle spring feeds, together with some other springs located a few hundred meters below, the Gavarnie waterfall (Fig. 1b). A tracer experiment (du Cailar et al., 1953) indicated that part of the water of the Gavarnie waterfall, and thus likely also from Brulle spring, comes from a ponor in the Lago helado (lake, Fig. 1e)~~,~~ located ~2.3 km to the east of Devaux cave (Figs. 1b and 2a). The Gavarnie waterfall (Fig. 1b) turned green within ~21 hours after injection of the tracer but the water at Brulle spring was not directly checked (du Cailar et al., 1953). During the colder months, the spring ~~water~~ as well as the Gavarnie waterfall freeze.

The geomorphology of the area is dominated by karst, glacial and periglacial landforms. The area was strongly glaciated during the last glacial period on both sides of the massif (e.g.~~,~~ Reille and Andrieu, 1995; Sancho et al., 2018b; Bartolomé et al., 2021). Today, only two glacier relicts covered by scree deposits are present in the Gavarnie cirque (Fig. 1b): 1) the Cascada dead-ice which is located several hundred meters below Devaux cave, and 2) a dead-ice accumulation in the NE wall of the cirque. Till present close to Brulle spring, on the access to Devaux and in the Cascada glacier, point to a much larger glacier

Con formato: Inglés (Estados Unidos)

extent in the past, maybe corresponding to the Little Ice Age or even the Neoglacial advance recognized in the nearby Tucarroya (Fig. 1b) and Troumouse cirques (Gellatly et al., 1992; González Trueba et al., 2008; García-Ruiz et al., 2014, 2020).

The study area lies at the transition between Atlantic and Mediterranean climate, with generally cold and dry winters and warm and dry summers. In MPm, the annual ~~zero~~ 0°C isotherm is located at ~ 2900 m a.s.l. (López-Moreno et al., 2016; Serrano et al., 2019). The wet seasons are fall and spring. The annual precipitation at the Góriz meteorological station (2150 m a.s.l. and 3 km SE of the cave) averages 1650 mm. However, mass balance calculations of the nearby Monte Perdido glacier, where more than 3 m of snow (density~~(p~~ 450 ~~Kk~~g/m^3) accumulates between November to April, indicates a minimum amount of 1500 mm ~~w.e (~~water equivalent~~)~~, therefore the total annual precipitation in ~~elevate~~high ~~areas~~parts of the massif exceed~~ss~~ 2500 mm ~~However, mass balance calculations of the nearby Monte Perdido glacier suggest that annual precipitation next to the cave may exceed 2500 mm, as the snow depth measured in early May exceeds on average 3 m~~ (López-Moreno et al., 2019). In the MPm, discontinuous permafrost is present between ~2750 and ~2900 m a.s.l. and becomes more frequent above ~2900 m a.s.l. on the northern side (Serrano et al., 2019). Periglacial activity is characterized by rock glaciers, solifluction lobes and patterned ground (Feuillet, 2011).

Con formato: Inglés (Estados Unidos)

Con formato: Inglés (Estados Unidos)

3. Material and methods

3.1 Cave survey and mapping

A survey of Devaux cave was conducted using a compass and clinometer as well as a laser distometer (Disto-X, Heeb, 2014). In addition to cave ice, chemical and clastic deposits were mapped in~~side~~ the cave~~. These features were overlain onto the cave survey to produce a geomorphological cave map~~ (Fig. 2b). The labelling of the cave chambers (A to K) follows the nomenclature introduced by Devaux (1929) and Rösch and Rösch (1935).

A map of potential solar radiation (RAD) of the MPm was obtained using an algorithm which considers the effects of the surrounding topography on shadowing considering the position of the sun. RAD was calculated for every month ~~of the year~~ and was then averaged to obtain an annual mean. Details of this computation can be found in Pons and Ninyerola (2008).

3.2 Cave monitoring

The cave consists of large rooms (e.g., room F, ~~or~~ and those located beyond SCAL chatière) connected by small galleries (Fig. 2b), locally with narrow passages (e.g., galleries close to SPD room or SCAL chatière, Fig. 2b). 15 stations were installed in the outmost ~350 m of the cave to monitor air (11 sensors), water (2 sensors) and rock temperature (2 sensors) (Fig. 2b). Cave air temperature variations were recorded using different devices (Hobo Pro v2 U23-001 (accuracy ±0.25°C, resolution 0.02°C), Tinytag Talk 2 (accuracy ±0.5°C, resolution, 0.04°C) and ELUSB2 (accuracy ±0.21°C, resolution 0.5°C)). The cave river temperature was recorded at two points. T~~;~~ ~~t~~he first site (W7) was located close to the Brulle spring (Fig. 2b; Hobo TiDBit V2, accuracy ±0.21°C, resolution 0.02°C) and, the second site (W6) was located in room F (Fig. 2b; Hobo UA-001-08; accuracy ±0.53°C, resolution 0.4°C). Both sensors were installed at a water depth of 20 cm. Finally, the rock temperature was recorded at two sites (R1 and R2 in room D and K, respectively) using a Hobo U23-003 device (accuracy ±0.25°C, resolution 0.02°C). Each sensor has two external temperature probes (channels 1 and 2, Ch1-Ch2). These temperature probes were installed in two horizontal drill holes of 60 cm depth, ~1.5 to 2 m from each other.

We monitored sporadically the cave during different ~~time~~ intervals between 2011 and 2015, while a continuous monitoring was carried out between July 2017 and July 2021. ~~We calculated the m~~Maximum, minimum and mean temperatures as well as the number of frost/warm days were obtained for each sensor and site (Fig. 2b). Changes in the ice morphology were evaluated using wall marks measured at four points since 2013 in room G and using one point during 2020-2021 in room SPD (Fig. 2b) using a digital sliding caliper.

The outside temperature was measured at ~~two points in the MPm, at~~ the “Porche” entrance (~2836 m a.s.l.) and on the southern face of MPM at ~2690 m a.s.l. For

Comentado [M11]: Reviewer #2
C) l183:

comparison, these temperature records were corrected assuming an adiabatic lapse rate of ~~0.55°C 100^{-1}~~5.5 °C km^{-1} ~~m~~ (López-Moreno et al., 2016; Navarro-Serrano et al., 2018) to an elevation of ~2850 m a.s.l., corresponding approximately to the lower limit of the hydrological catchment area of Devaux. In both cases, the temperature was measured using Tinytag Talk 2 sensors equipped with a radiation shield. These data were compared to the temperature record from the Pic du M~~m~~idi de Bigorre meteorological station (PMBS; 2011-2020) (2860 m a.s.l., ~28 km N of Devaux) obtained from Météo-France. Moreover, the homogenised ~~MAAT~~ data~~set~~ available since 1882 from PMBS (Bücher and Dessens, 1991; Dessens and Bücher, 1995) ~~was~~ were used to ~~identify~~ identify long-term ~~climatic~~ temperature trends.

3.3 ~~Mineralogy, water and mineral sampling~~ X-ray diffraction, ion chromatography and sulfur isotopes

X-ray diffraction (XRD) analyses were performed on sulfate and carbonate crystals from rooms G, D and K, as well as on sulphide and oxidized crystals thereof from the host rock (Fig. ~~s~~S1). The analyses were performed at the Geosciences Institute in Barcelona (GEO3-BCN-CSIC) using a Bruker-AXS D5005 powder diffractometer configured in θ/2θ-mode (e.g. ~~(~~Rodríguez-Salgado et al., 2021)~~theta-2 theta geometry~~.

Samples of cave drip~~s~~ water, ice and river water were analysed for major ions by ion chromatography (IC) at the laboratories of the Pyrenean Institute of Ecology (Zaragoza). Carbonate alkalinity was determined by titration within 24 hours after sampling.

Sixteen samples, including sulfate crystals, dissolved sulfate and pyrite crystals were selected for sulfur isotope analysi~~e~~s at the Godwin Laboratory for Paleoclimate Research of the University of Cambridge (UK), following the methodology of ~~(~~Giesemann et al., (1994). For gypsum samples, ~5 mg of powdered gypsum were dissolved in deionized water at 45ºC overnight. Then, a $BaCl_2$ solution (50 g/L) was added to induce $BaSO_4$ precipitation. In the case of water samples, $BaCl_2$ was added directly to the sample. Subsequently, 6M HCl was added to remove any co-precipitated carbonate minerals~~s~~ and the $BaSO_4$ precipitate was rinsed several times with deionized water. Finally, $BaSO_4$ was

Comentado [M12]: Reviewer #1
line 210: I suggest expressing the lapse rate as 5.5°C km^{-1} because the current expression is confusing. It suggests 0.55°C change by 0.01 m.

Comentado [M13]: Reveiwer #1

line 214: Please capitalize "Midi"

Comentado [M14]: Reviewer #1:
The title of sub-section 3.3 needs revision. The current title is misleading. The section is not about sampling but about the methodology of the applied mineralogical and geochemical analyses.

Comentado [M15]: Reviewer #1:
An additional related comment is that it is stated in section 4.4.2 that "*XRD analyses yielded …gypsum, calcite, … pyrite and goethite*," however no evidence is presented. I suggest adding some annotated diffractograms (at least in a supplementary document) in the revised version.

Comentado [M16]: Reviewer #1
line 244: Maybe "Bragg-Brentano geometry" or "θ/2θ-mode" would be the appropriate expression.

Comentado [M17]: Reference added.

Rodríguez-Salgado, P., Oms, O., Ibáñez-Insa, J., Anadón, P., Gómez de Soler, B., Campeny, G., and Agustí, J.: Mineralogical proxies of a Pliocene maar lake recording changes in precipitation at the Camp dels Ninots (Pliocene, NE Iberia), Sedimentary Geology, 418, 105910, https://doi.org/10.1016/j.sedgeo.2021.105910, 2021.

Con formato: Color de fuente: Énfasis 1

Código de campo cambiado

Comentado [M18]: Reviewer #1:
It is also quite strange that there is not any reference for the applied methods. Please consider citing the proper references in the revised manuscript.

Comentado [M19]: Reference added:

Giesemann, A., Jaeger, H.-J., Norman, A. L., Krouse, H. R., and Brand, W. A.: Online Sulfur-Isotope Determination Using an Elemental Analyzer Coupled to a Mass Spectrometer, Anal. Chem., 66, 2816–2819, https://doi.org/10.1021/ac00090a005, 1994.

dried at 45ºC overnight. Sulfates dissolved in water were precipitated using the same method.

Isotope measurements were carried out using a Flash Elemental Analyzer (Flash-EA) at 1030 ºC. The samples were folded in tin capsules. After sample combustion, the generated SO_2 was measured by continuous-flow gas source isotope ratio mass spectrometry (Thermo Scientific, Delta V Plus). Samples were run in duplicate and calibration was accomplished using NBS-127. The reproducibility (1σ) of $\delta^{34}S$ was better than 0.2‰, similar to the long-term reproducibility of the standard over the run (0.2‰). $\delta^{34}S$ isotope values are reported relative to VCDT (Vienna-Canyon Diablo Troilite).

4. Results

4.1 Devaux cave description

Devaux cave is ~2500 m long and comprises three distinct levels (Fig. 2b). The lower and the middle levels correspond to the Brulle spring (0 m), and the "Porche" entrance (~+14.5 m), respectively. The third one comprises chambers and galleries +21 m to +29 m above the Brulle spring (Fig. 2b). In the inner part of the cave, some unexplored vertical chimneys may connect to sinkholes in the catchment above the cave (Fig. 2a). The main ice deposits are located in rooms D, G, SPD and K (Fig. 2b). Except for SPD, these chambers located above the Porche entrance (between ~+1 and +7 m) can be accessed via ascending passages.

During the cold season, the cave river starts freezing at the spring and the ice then expands backward into room F (Fig. 2b). The ice totally or partially clogs the main gallery and dams the water inside the cave forming a small lake (cf. also Rösch and Rösch, 1935). This process is important for the seasonal ice extent as the flooding of the cave depends on whether the springs (North 1 and North 2) are frozen or not (e.g., Rösch and Rösch, 1935). Webcam observations (Gavarnie, Oxygène hut) suggest a possible freezing of the Brulle spring from late November to mid-May simultaneous with the freezing of the Gavarnie waterfall. Moreover, historical photos (e.g., Devaux, 1929; Rösch and Rösch, 1935) and our own observations show that snow during winter and spring can

reach the Brulle entrance - a situation that also favours the blocking of the springs. As a result of such flooding events, slackwater deposits ~~are present~~formed in the cave entrance zone, but locally also further into the cave (e.g., in rooms I, J, K and SCAL chatière, along the main gallery; Fig. 2b), while silty sediments are found at elevated positions with respect to the river level (e.g., in rooms D and G). Sandy sediments dominate in the large rooms located beyond the SCAL chatière. Two such successions (~1 m thick) comprising hundreds of rhythmitic fine -sand~~-~~ and silt layers are present in elevated areas with respect to the current river, witnessing major events of back-flooding.

Observations made during summer show a dominant air-flow direction from the inner to the outer parts of the cave, exiting through the Brulle and Porche entrances. Conversely, the opposite is expected for the cold season (chimney effect). When the Brulle spring is partially clogged by ~~the~~ ice during early summer forcing the stream to flow below the ice, air flows from room F to C (Fig. 2b) (e.g., summer 2021). The air flow is imperceptible in rooms D, G, and close to K located away from the main cave passages.

4.2 Climate setting of Devaux cave

The MAAT at the elevation of Devaux cave is ~0 ºC (-0.04 ºC; 2017-2021). On the other hand, a positive MAAT (1.8 ºC) is recorded on the southern side of the MPm at a similar altitude (Fig. 3a). Maximum and minimum air temperatures outside the cave vary between 24.5 °C and -17.2 °C (hourly values, 2017-2021). The PMBS MAAT record (Fig. 3b) shows a~~n increase~~ warming trend of ~~~+~~around +1.5 ºC since the beginning of the measurements in 1882. Before 1985, temperatures below 0ºC dominated the annual cycle, while positive MAATs became more frequent in recent years. Minimum temperatures also show a~~n temperature~~ increase~~e~~ing trend of ~+2.5 ºC, while the maximal annual temperatures do not show a clear trend. The north-facing Gavarnie cirque is associated with a clear RAD anomaly (Fig. 4). Values lower than 215 kWh/m^2 are observed at ~2000 m and between ~2800 and 2900 m a.s.l., corresponding to the cirque bottom, the area located behind La Torre peak and the surroundings of Devaux cave. At the cave ~~site~~ entrance the RAD value is only 390 kWh/m^2, in

Comentado [M20]: Reviewer #2

line 290: Please explain it a bit more what is "an increase of ~+1.5 ºC". A trend value? or the difference between the mean of a certain period at the beginning and at the end of the record? or what?

Comentado [M21]: Reviewer #2

line 299: Please check the dimension.

stark contrast to the summit areas and surroundings where the RAD often exceeds 1500 kWh/m^2 (Fig. 4).

While the mean daily air temperature (MDAT) at the cave entrance (purple line in Fig. 5) and the temperature series from PMBS (pink line in Fig. 5) agree in their absolute values, the variability of MDAT at the Devaux entrance is lower than at the PMBS. This pattern could be related to local topographic conditions leading, for instance, to less RAD, or to the position of the sensor in the cliff (less night emissivity). Given this radiation contrast, warmer temperatures prevail on the southern side of the MPm (Fig. 4), favouring early snowmelt in spring and early summer, while at the same time the temperature stays below 0 ºC in the cave's surroundings.

4.3 Devaux cave temperature variations

The cave can be separated into distinct areas depending on their thermal regime: ventilated galleries (rooms A, B, C, F and the main gallery from SPD to SCAL chatière) ~~to K~~) and ~~those~~ poorly ventilated parts off the main air flow path (rooms D, G, K - Figs. 2b, 5).

4.3.1 Well-ventilated cave parts

Air ($T2_{air}$, $T5_{air}$, $T10_{air}$, $T11_{air}$) and water ($W6_{water}$, $W7_{water}$) temperature data show large seasonal oscillations ~~at $T2_{air}$, $T5_{air}$, $T10_{air}$ $T11_{air}$, $T12_{air}$, $W6_{water}$, $W7_{water}$ and $R2_{rock}$ sensors.~~ All sensors except $T11_{air}$~~,~~ ~~$T12_{air}$, and $R2_{rock}$~~ show a few days ~~with~~ of positive temperatures during summer. Sensor $T2_{air}$ (2011-2012, Fig.5a), which is also the closest to the Porche entrance, shows the highest correlation (r) with the external temperature (0.73, p<0.001). Sensor $T5_{air}$ (2017-2021, Fig. 5d) in room B also shows a high correlation and significant correlation (0.82, p<0.0005) with the outside temperature. During the major cave ~~refrigeration~~cooling that takes place between the end of October ~~to~~and May and the correlation is significa~~t~~ent and ranges between 0.68 to 0.84. During ~~the~~ summer~~s~~ and part of ~~the~~ fall~~s~~, the correlation~~s~~ decreases notably (-0.23 to 0.76). Sensor $T11_{air}$ (2018-2021, Fig. 5d) ~~is located in SPD room. Despite being a well-ventilated gallery, the sensor is relatively protected from the air flow by the room morphology and shows lower correlations (0.69, p<0.001)~~is partly protected from the air flow and shows lower a correlation (0.69, p<0.001) despite being located in a well-ventilated

Comentado [M22]: Reviewer #2
l315: I think this could be reformulated, as the authors list water, and rock T sensors together with the air T sensors.

Con formato: Color de fuente: Automático

Con formato: Color de fuente: Automático

gallery (SPD room). Also during the ~~refrigeration~~winter months, the correlations are lower (0.49-0.62, p<0.001) than in T5air. ~~Sensor T5$_{air}$ (2017-2021, Fig. 5d) in room B also shows a high correlation with the outside temperature from November to May (0.82, p<0.001(2017-2018); 0.66, p<0.001(2018-2019); 0.66, p<0.001(2019-2020); 0.86, p<0.001(2020-2021)), while during summer and fall correlations with external temperatures are slightly weaker (0.52, p<0.001(2017-2018); 0.37, p<0.001(2019-2020); 0.66 p<0.001(2020-2021)). Sensor T11$_{air}$ (2017-2021, Fig. 5d) is located in SPD room. Despite being a well-ventilated gallery, the sensor is relatively protected from the air flow by the room morphology and shows lower correlations (0.45, p<0.001(2018-2019); 0.34, p<0.001(2019-2020); 0.79 p<0.001 (2020-2021)) compared to T5$_{air}$.~~ Sensor T10 (2014-2015, Fig. 5c) does not show any significant correlation with the external temperature. ~~Sensors T12$_{air}$ and R2$_{rock}$ are located in room K, and similar to T11$_{air}$, the chamber morphology shields them from the air flow. Rock temperature sensor R2 $_{rock}$ shows a slightly variable temperature ranging between -0.19°C and -0.28°C (mean of -0.24 and -0.23°C for channel 1 and 2, respectively). Sensor T12$_{air}$ shows a low correlation with the external temperature (r^2=0.35, p<0.001 (2018-2021)), and the same is observed for T$_{ext}$ – R2$_{rock}$ (r^2=0.35, p<0.001 (2019-2021). Meanwhile the correlation between T12 $_{air}$ and R2 $_{rock}$ is high but not significant (r^2=0.93, p>0.005 (2019-2021).~~

~~The water s~~Sensors W6$_{water}$ and W7$_{water}$ (Figs. 5b, c) recorded water temperature variations during the years 2012-2013 and 2014-2015, respectively. Both sensors record a continuous temperature decline from the end of November to mid-January until the water freezes. At W7$_{water}$, the temperature ranges between -0.3 and -5.8 °C between the end of fall and the beginning of winter, while ~~between January and the beginning of June,~~ the temperature stays close to 0°C between January and the beginning of June. At W6 $_{water}$, the temperature reached a minimum of -1.7 ºC and shows smaller variations than at W7$_{water}$. No significant correlation was found between the external air temperature and the river water temperature. Only W6$_{water}$ shows a weak ~~small~~ correlation with the external temperature when ice is absent (0.39 p<0.001 and 0.40 p<0.001).

Comentado [M23]: line 346: I suggest replacing "small" with "weak".

For each monitored interval, the mean annual cave temperature at the T2$_{air}$, T5$_{air}$ and T11$_{air}$ sensors is lower than the outside mean temperature ~~for the same~~

period (by 0.4º, 2.0º, 3.3º C lower, respectively). The W6$_{water}$, W7$_{water}$ and T10$_{air}$ sensors show mean temperatures higher than the external mean temperatures (by 1.6º, 2.6º, 2.5º C higher, respectively). The periods 2011-2012 and 2017-2018 (at T2$_{air}$ and T5$_{air}$, respectively) represent the coldest cave years of the monitoring period.

4.3.2 Poorly ventilated cave parts

Air temperature sSensors located in rooms D (T3$_{air}$, T4$_{air}$, T8$_{air}$, R1$_{rock}$), and G (T9$_{air}$), K (T12$_{air}$,) and rock temperature (R1$_{rock}$, R2$_{rock}$) show air temperatures below 0 ºC during the monitoring period with small oscillations and a weak and/or insignificant correlation with the external air temperature. All sensors show temperatures below 0 ºC during the monitoring period with small oscillations. Sensor R1$_{rock}$ (Fig. 5) recorded rock temperatures consistently below 0ºC during the entire monitoring period. This sensor shows constant rock temperatures (-1.24 °C and -1.27 ºC for channels 1 and 2, respectively), similar within error to the cave air temperature (T3$_{air}$, T9$_{air}$; 2019-2021). All sensors except for T3$_{air}$ (2011-2012, Fig. 5a) show mean air and rock temperatures lower than the mean external temperature during the same period (by 0.59 °C to 2.47ºC lower). The muted temperature variations in these chambers reflect reduced heat exchange compared to the well-ventilated parts of the cave. Sensors T12$_{air}$ and R2$_{rock}$ are located in room K, and similar to T11$_{air}$, the chamber morphology shields them from the air flow. Rock temperature sensor R2$_{rock}$ shows a slightly more variable temperature ranging between -0.19°C and -0.28°C (mean of -0.24 and -0.23°C for channel 1 and 2, respectively). Sensor T12$_{air}$ shows a low correlation with the external temperature (r^2=0.35, p<0.001 (2018-2021)), and the same is observed for T$_{ext}$ - R2$_{rock}$ (r^2=0.35, p<0.001 (2019-2021). Meanwhile the correlation between T12$_{air}$ and R2$_{rock}$ is high but not significant (r^2=0.93, p>0.005 (2019-2021).

Comentado [M24]: Reviewer #2
l357: I think R1 could be dropped from the list in parentheses, as it is not an air temperature sensor.

4.4 Cave deposits

414 **4.4.1 Ice**

415 Congelation ice formed by freezing of water within the cave is the most abundant
416 type of ice, and four main ice deposits are located in chambers D, G, SPD, and
417 K (Fig. 2b). The most relevant feature of these ice bodies is their high
418 transparency and massive aspect, i.e. the lack of layering (Figs. 6a, b).
419 Transparent ice is present on the ceiling, blocking chimneys, galleries and
420 fractures. The local loss of transparency is related to the presence of cryogenic
421 cave minerals and/or air inclusions (Figs. 6a, b, c, d).

422 A highly transparent ice deposit covers the southwest wall of room D and blocks
423 the access to a gallery (Fig. 6a). The height of this deposit reaches ~6 m, and its
424 base is located ~20 m above the Brulle spring. The thickness of this ice deposit
425 ranges from 4.5 to 14.5 m (horizontal laser measurements across the ice in the
426 gallery blocked by ice) and the estimated volume ranges from ~350 to ~710 m^3.
427 Three unconformities marked by cryogenic minerals were identified in this ice
428 body.

429 In room G, an ice body (~25.8 to 29.6 m above the Brulle spring) is present on
430 the ceiling (Fig. 6b) and the estimated ice volume is ~180 m^3. A comparison with
431 a historical photograph shortly before 1953 (Casteret, 1953) suggests that the ice
432 body has not changed significantly during the last ~69 years (Figs. 7a, b). Ice-
433 rock distances measured at four points, however, reveal small changes at three
434 of them. The first has retreated 9.8 mm since 2014 (mean 0.9 mm a^{-1}, n=2), the
435 second has retreated 19.2 mm since 2014 (mean 0.6 mm a^{-1}, n=5), and the third
436 one has retreated 15.8 mm since 2013 (mean 2.2 mm a^{-1}, n=7). At ~80 m from
437 the entrance, a small descending room (SPD) (Figs. 2b, 6c) hosts a small volume
438 of ice. Measurements between 2020 and 2021 indicate a retreat of 20 mm a^{-1}
439 (n=1). A last major ice deposit is present ~280 m from the entrance (room K),
440 where transparent and massive ice (~15.5 m above the Brulle spring) ~~is~~ currently
441 fills a ~~filling a~~ cupula or chimney (Figs. 2b, 6d). Additional ice bodies are present
442 behind the SCAL chatière in the upper gallery (Fig. 2b), but they have not been
443 studied.

444 In contrast to these massive ice deposits, layered ice of seasonal origin is present
445 in small chambers adjacent to the river (E and F rooms) (Fig. 6e). This ice forms

Comentado [M25]: Reviewer #2
l396: (T) transparent and massive ice (~15.5 m above the Brulle spring) currently fills a cupula or chimney

sheets of ~~around~~ about 10-15 cm in thickness which are present in room F and nearby areas (Fig. 6f). This ice is related to the damming and freezing of water inside the cave when the Brulle spring freezes. Our visits from 2017 to 2021 revealed that most of the damming and subsequent ice formation in room F took place during winter and spring 2017-2018 corresponding with the coldest months (both inside the cave and outside) of the monitoring period (Fig. 5d). These ice slabs are characterized by flat surfaces on both sides and obviously record incomplete freezing of the dammed water. The ice sheets largely disappeared during summer and fall, and only strongly degraded ice remained in elevated areas of room F.

On the other hand, ~~the~~ ice sheets associated with earlier episodes of river damming and freezing have disappeared, and only linear colour changes remained as witnesses of such events on the walls of the room E (Fig. 8d). A historical photograph exemplifies these ice levels in the access between rooms F and E (Fig. 8a). In August 1984 the ice was close to the ceiling and nearly 1 m thick (Fig. 8a; Marc Galy, pers. comm.). This contrasts with the low ice level in recent years (Fig. 8b). In total, three ice-level marks were identified in relation to back-flooding and subsequent freezing of ponded water (Figs. 8c, d). They appear at a lower elevation than the Porche entrance (c.+9.5, +9.2, +8.8, m with respect to the Brulle spring).

Another important feature is the presence of hoarfrost, which ~~is~~ was observed in room A, B, F and along the gallery between SPD and ~~K~~ J (Figs. 2b, 7g, ~~7~~h). The crystal size varies from few mm to 4 cm and appears to be upholstering some galleries and cupolas, forming aggregates that hang from the ceiling (Fig. 6h). Finally, seasonal ice formations (e.g., icicles and ice stalagmites), as well as drips are restricted to the outmost ~15 m, in the vicinity of both entrances, and in the innermost part of the cave (~ 500 m from the entrance). Seasonal ice formations are absent in cave sectors where transparent ice bodies and hoarfrost are present. Firn deposits derived from snow are restricted to the Porche entrance.

4.4.2 Mineral deposits

They comprise mainly cryogenic cave minerals. XRD analyses of samples from rooms D, G and K yielded gypsum and calcite, while the sulfide crystals and their oxidation products present in the host rock were identified as pyrite and goethite, respectively. The presence of cryogenic gypsum in Devaux was already reported by du Cailar and Dubois (1953). In room D, gypsum was observed within the ice and on boulders (Figs. 9a, b, c). A total of three gypsum levels (lower, middle and upper, located at ~21.4, ~22.6 and ~23.9 m, respectively, with respect to the Brulle spring) were identified in the ice (Fig. 9a). Due to the progressive retreat of the ice body, some of these crystals are now present on the ice surface. Gypsum levels comprise large single crystals (0.5-1 cm in diameter), aggregates forming rafts (10 cm) up to 1 cm in thickness (Fig. 9b), as well as a fine crystalline fraction. ~~Visual e~~Examination of the fine fraction ~~under~~ using a binocular stereo microscope indicates the presence of ~~small aggregates of~~ cryogenic cave carbonates and gypsum (CCG) ~~(<1 mm)~~ including globular, single and twin morphologies <1 mm in diameter (Fig. 9d).

In room G, gypsum and carbonates crystals are present in the lower part of the ice deposit (Fig. 10e) and on blocks. There, CCC are larger (>10 mm) than in room D and include globular shapes and raft-like aggregates, similar to those reported by Žák et al. (2012). Some of these CCC show gypsum overgrowths (Fig. 9f). Across the ice surface, patches of globular CCC (sub-millimeli~~l~~tre size) have been released by ice sublimation (Figs. 7a, b). In room SPD, CCC and CCG (≤ 2 mm) are present within and on the ice (Figs. 2b, 7c). Finally, in room K, only few CCC were still present within the ice, while most of them form heaps of loose crystals covering blocks. Some of these CCC~~s~~ exceed 5 mm in diameter. Crystal morphologies include rosettes, skeletons and rhombohedrons similar to those reported by Žák et al. (2012) as well as white tapered crystal aggregates. Beyond room K, regular carbonate speleothems (i.e. stalagmites, stalactites and flowstones) are present. ~~On the contrary, g~~Gypsum ~~crystals growing~~coating ~~from~~ walls or ceilings w~~ere~~as not observed.

4.5 Cave water chemistry and sulfate isotopic composition

Comentado [M26]: Reviewer #2
l452: (T, American English spelling) millilitre

Comentado [M27]: Reviewer #2
l453: (T) in room SPD, CCC and CCG

Comentado [M28]: Reviewer #2
l456: for the sake of consistency, I would drop the s at the end of CCC here.

Comentado [M29]: Sentence added:

On the contrary, Gypsum coating walls or ceilings was not observed.

The chemical composition of water in Devaux cave ~~(n=22) cave~~ is dominated by calcium and bicarbonate with relatively high Mg concentrations and locally also elevated sulfate concentrations (Table 1). Total dissolved solids (TDS, n=7) vary from 57 to 315 mg l^{-1}. Devaux´s dripwater has higher mean sulfate concentrations (65 mg l^{-1}) than the cave river (11 mg l^{-1}) and massive and seasonal ice (2.8-18 mg l^{-1}). ~~Concerning the sulfur isotopic composition (Table 2), the~~ The $\delta^{34}S$ value of dissolved sulfate in the dripwater is -14.4‰ (n=1), which is significantly higher than in cave river water (-28.5‰ to -27.3‰, n=2; Table 2). Gypsum crystals in room D show ~~homogeneous~~ $\delta^{34}S$ values ranging from -15.1‰ to -15.8‰ (n=7), while in room G they range from -12.3‰ to -11.9‰ (n=5). A pyrite sample from the host rock yielded a $\delta^{34}S$ value of -12.7‰ (n=1).

5. Discussion

5.1. Processes controlling the thermal regime in Devaux cave and the extent ~~current~~ of permafrost ~~extent~~

A complex spatial distribution and a high degree of heterogeneity are among the main characteristics of mountain permafrost (Gruber and Haeberli, 2009). In Devaux cave the existence of permafrost can be related to a combination of two processes: i) cave atmospheric dynamics, and ii) conductive heat transfer through the rock.

Devaux cave is characterized by mean air and rock temperatures lower than the external mean annual temperature (Fig. 5). The low cave temperatures in winter lead to an inward airflow and an associated negative thermal anomaly behind the ~~cave~~ entrance zone. On the contrary, during summer~~,~~ the cold and dense air flows out of the cave due to the temperature difference between outside and inside air. ~~Also t~~The heat supplied to the cave by the river ~~can~~ also ~~modify~~influences the cave air temperature by exporting thermal energy ~~. Thus, this process drags cold outside air into~~from the cave during winter ~~and on the contrary during summer. Devaux cave is characterized by mean air and rock temperatures lower than the external mean annual temperature (Fig. 5). The low cave temperatures in winter lead to an inward airflow and an associated negative thermal anomaly behind the cave entrance zone.~~ Similar seasonal ventilation

Comentado [M30]: Reviewer #2

E) l315 - figure 5d, the air temperature variations at T11 and T5 (and T2) could be discussed in additional detail (at line 481 for instance).

patterns have been observed in ice caves elsewhere (e.g., Luetscher et al., 2008; Colucci and Guglielmin, 2019; Perşoiu et al., 2021).

On the other hand, positive temperatures are observed both in the cave river and in the air at the ~~cave~~ entrance (Fig. 5), reflecting heat advected by water (river) and the influence of the external temperature (cf. Luetscher et al., 2008; Badino, 2010). The lack of correlation between the external and internal temperatures and the small temperature variability in rooms D, G, and K reflect their thermal isolation from well-ventilated cave parts. There, the apparent thermal equilibrium between the rock and the cave atmosphere (T_{rock}=T_{air}) supports the notion that heat exchange is dominated by conduction through the bedrock.

The MAAT at the altitude of the cave is -0.04 ºC (2017-2021) suggesting that the 0 °C isotherm is located close to the cave. Using an array of techniques (geomatic surveys, temperature monitoring, temperature at the base of the snowpack (BTS) and geomorphological and thermal mapping), Serrano et al. (2019) ~~found~~ observed mean annual ground temperatures between -1 and -2 ºC on the northern slope of the MPm suggesting that discontinuous permafrost is present between 2750-2900 m a.s.l., with more continuous permafrost startings ~~s~~ at 2900 m a.s.l. The orientation of the Gavarnie cirque, as well as the high slope angle, and shadow from the surrounding peaks favour the preservation of permafrost at lower elevations (e.g., Gubler et al., 2011).

Given the high thermal inertia of the rock, the permafrost temperature at depth is still under the influence of past climate conditions (e.g., Haeberli et al., 1984; Noetzli and Gruber, 2009) and, therefore, part of the current permafrost in the area could be inherited from previous colder times (e.g., Colucci and Guglielmin, 2019). In particular, the low mean annual temperatures recorded at PMBS ~~at~~ in the late 19th century ~~the beginning of the Industrial Era are~~ were favourable conditions for permafrost development ~~in the recent past~~. We surmise that the current permafrost could be inherited from colder periods of the Little Ice Age.

In well-ventilated ice caves hoarfrost is the most dynamic ice formation on seasonal time scales. The presence of perennial hoarfrost is, however, indicative of a continuously frozen bedrock and thus representative of caves within the

Comentado [M31]: Reviewer #2
l501: (T) with more continuous permafrost starting at 2900 m asl

Comentado [M32]: Reviewer #2

D) l506-513

Comentado [M33]: Reviewer #1.

line 511: I suggest replacing the term "beginning of the Industrial Era" with "late 19th century". As far as I know the Industrial Era begun much earlier than the PMBS record.

permafrost zone (e.g. Luetscher and Jeannin, 2018; Yonge et al., 2018). In Devaux cave, perennial hoarfrost is observed in rooms where the bedrock is surrounded by small ice bodies (e.g., gallery close to SPD room, Fig. 6g). On the other hand, seasonal hoarfrost is present in ventilated galleries (A, B, C, F and between SPD and J). Seasonal hoarfrost in room B and C, and in the area between H to J, disappears at the end of summer, probably because of the heat delivered by the cave river, as recorded by the T5 sensor (Fig. 5).

The presence of permafrost in Devaux's catchment is supported by the absence of drips and/or seepage in the investigated cave passages (e.g., Luetscher and Jeannin, 2018; Vaks et al., 2020). Active drips and seasonal ice formations are limited to the first ~15 m of the cave as well as to the inner part (beyond room K). Mountain permafrost thus penetrates ~350 m longitudinally from the ~~East~~ eastern cliff of the Gavarnie cirque to the southern side of the massif~~, following a west-east direction~~. On the other hand, given the elevation of the cave and the ~~topographic~~ topography ~~relief~~ above the cave, the current maximum permafrost thickness ~~(without taking into account the active layer)~~ on the southern side of the MPm is ~200 m (without taking into account the active layer).

5.2. The origin of ice in Devaux cave

The transparent and massive character of Devaux´s cave ice, as well as the presence of CCC, which formation requires low congelation rates (Žák et al., (2004)), suggests that this ice formed by slow freezing of water dammed by ice at the spring. This model is consistent with the climate ~~in~~ of the Gavarnie cirque, cave geomorphological observations, cave air and water temperatures as well as historical reports. The cave water level can rise by several meters as indicated by slackwater deposits upstream of the Brulle spring.

Comentado [M34]:
Reviewer #2
l535-536: massive ice is formed by slow freezing - there should perhaps be a reference here.

The distribution and characteristics of ice bodies in Devaux cave indicate that the hydraulic head rose by at least ~ 15 - 29 m, which is the elevation of the ice bodies in rooms G, F and K. This situation requires that all springs (including Porche) are blocked for a sufficiently long time to allow for complete freezing of these cave lakes. The lack of important unconformities in this massive ice (e.g., detrital

layers), which are usually related to seasonal ablation (e.g., ~~(~~Luetscher et al., 2007; Stoffel et al., 2009; Hercman et al., 2010; Spötl et al., 2013), suggests that the ice deposit in room G it is the result of a single flood event. On the contrary, the small unconformities recognized in the ice body in room D suggest that several cycles of damming and subsequent ice formation cannot be discarded in the formation of this ice deposit.

~~Our~~ These observations indicate that under the current climate (both in the cave and outside) only part of the water dammed in rooms F and E freezes during winter and spring. This strongly suggests that the ice bodies in Devaux cave must have been associated with colder and/or longer events of ponding and freezing than today, when the cave was effectively sealed from the outside for prolonged times. We hypothesize that the advance of a glacier on the steep slopes of Devaux's surroundings could have contributed to the blockage of the spring, leading to backflooding and the formation of large ice bodies in the cave. In the study area, such periods of glacier growth occurred during the Little Ice Age and/or the Neoglacial (González Trueba et al., 2008; García-Ruiz et al., 2014, 2020).

The freezing of a flooded cave passage cannot be explained by the advection of cold air alone. It is thus surmised that heat transfer through the host rock is a more plausible mechanism for the complete freezing of ~~the~~ ponded water. The cave ice bodies~~,~~ ~~just as~~as well as the presence of cryogenic minerals~~,~~ therefore ~~represents a~~ record ~~of~~ a long cold period or ~~of~~ several ~~such~~ shorter episodes. Although ~~the~~ cryogenic minerals and in particular CCC_{coarse} are typically associated with permafrost thawing during warm spells (Žák et al., 2004; Richter et al., 2010; Žák et al., 2012; Luetscher et al., 2013), permafrost conditions prevailed during ice formation in Devaux cave. ~~Thus, T~~the water that feeds Devaux's springs infiltrated during late spring and summer from ponors at Lago helado and/or surrounding poljes~~. (which may have acted as local taliks).~~ However, the heat supplied by this water may have probably not been enough to thaw the frozen host rock. It is thus very likely that the hostrock temperature was

Comentado [M35]: Reviewer #1

lines 546-552: Discordancy without visible detrital layer could also indicate unconformity. A nice example can be found in Fig5 of Hercman et al., 2010 (http://www.geochronometria.pl/pdf/geo_36/Geo36_05.pdf). This type of discordancy/unconformity could be also considered in this part of the discussion.

Comentado [M36]: Reference added:

Hercman, H., Gąsiorowski, M., Gradziński, M., and Kicińska, D.: The First Dating of Cave Ice from the Tatra Mountains, Poland and its Implication to Palaeoclimate Reconstructions, Geochronometria, 36, 31–38, https://doi.org/10.2478/v10003-010-0016-2, 2010.

Comentado [M37]: Reviewer #1:

line 554: Maybe "These" instead of "Our".

Comentado [M38]: Reviewer #2

l568: (T) The cave ice bodies [...] therefore represent

Comentado [M39]: Reviewer #2:

lines 574-575: I suggest omitting the bracketed comment.

much lower and/or the outlets remained closed for longer periods than today to allow for the complete slow freezing of the ponded water.

5.2.1 Ice volume changes

The colour changes in the walls close to the river (room E), the historical photograph as well as speleological reports point to large changes (several meters) of in the height of the seasonal ice in the flood-prone sector of the cave (Figs. 8a, b). This ice is influenced by the heat exchanged between the water and the cave.

In contrast, changes in the ice volume are almost negligible in rooms D and G where the temperature is more constant and below 0ºC (Figs. 7a, b). The ice body in room G has been retreats retreating only by only ~0.6 to ~2.2 mm a^{-1}. A similar value (3 mm a^{-1}) was observed in Coulthard cave (Alberta, British Columbia, Marshall and Brown, 1974), a cave located within permafrost (Yonge et al., 2018). Changes in the ice body in this cave were related to slow sublimation due to convective air flow inside the cave (Marshall and Brown, 1974). On the other hand, the ice in SPD room shows higher ice retreat rates (~ 20 mm a^{-1}). Similar sublimation rates have been reported in ´others ice caves in the Pamir Mountains and the northern part of the Russian Platform (Mavlyudov, 2008; Žák et al., 2018). Overall, Devaux's cave ice deposits show a remarkable stability which contrasts to with the rapid changes observed in ice caves outside permafrost areas (Kern and Perşoiu, 2013; Perşoiu et al., 2021; Wind et al., 2022), including other ice caves in the Pyrenees and Picos de Europa (Belmonte-Ribas et al., 2014; Gomez-Lende et al., 2014, 2016).

Comentado [M40]: Reviewer #2
l596: (T) which contrasts with

Con formato: Inglés (Estados Unidos)

5.3. Cryogenic cave minerals

In Devaux cave, CCC and CCG are still present within the ice (Figs. 6, a, b, c, d). Worldwide, only very few *in situ* observations of coarse-grained cryogenic cave minerals are known (e.g., Bartolomé et al., 2015; Colucci et al., 2017). du Cailar and Dubois (1953) reported the presence of gypsum crystals at ~50 cm depth

within the ice in Devaux cave. The first evidence of *in situ* CCC_{coarse} in cave ice was reported from Sarrios 6, an ice cave at 2780 m a.s.l. on the southern slope of the MPm (Bartolomé et al., 2015). Colucci et al. (2017) documented the presence of CCC_{coarse} in a small ice cave in the Italian Alps. Recently, Munroe et al. (2021) found CCC_{coarse} in ice of Winter Wonderland cave (Utah, USA). Because of the abundance of cryogenic cave minerals, the size of individual crystals and aggregates thereof, and their ~~varied~~ different mineralogy, Devaux cave provides an additional opportunity for studying the origin of such cryogenic cave minerals.

~~The~~ CCG~~s~~ in Devaux cave represents, to our knowledge, the first occurrence of its kind in a carbonate karst terrain. So far, CCG~~s~~ have only been reported from gypsum karst areas in Russia and Ukraine (Korshunov and Shavrina, 1998; Žák et al., 2018 and references therein). In those ~~areas~~caves, tiny gypsum crystals ~~(gypsum powder)~~ form during rapid freezing of water. When ice sublimates in winter, ~~this~~ these ~~gypsum~~ particles ~~powder is~~are released and accumulate~~s~~ as powdery deposits on the ice surface. Eventually, they partly ~~powder~~ dissolve~~s~~ ~~on the ice surface~~ during spring and summer due to the increase in cave air humidity, and later recrystallize~~s~~ forming a wide variety of ~~delicate~~ crystal morphologies. CCG~~s~~ from Devaux cave show~~s~~ features that do not correspond to those previously published from gypsum karst caves. In particular, the Devaux cave CCG~~s~~ i) appear~~s~~ together with CCC_{coarse} crystals (≥5 mm in some cases, in rooms D and G), ii) the (raft-like) gypsum crystals are large (Fig. 9b) and, in some cases, are still found within the ice (Fig. 9a) and surrounded by milky ice rich in air inclusions (Fig. 9a, e), and iii) boulders are locally overgrown by gypsum (Fig. 9c).

Coarse-grained cryogenic cave minerals form in a semi-closed system, when ~~the~~ water freezes very slowly ~~freezes inside the caves at low freezing rates~~ (Žák et al., 2004). Once supersaturation is reached, CCM start to crystallize. The formation of gypsum crystals requires the presence of elevated concentrations of dissolved sulfate which may relate to i) sedimentary gypsum deposits intercalated within carbonates (e.g., Sancho et al., 2004), ii) the presence of hydrothermal water containing H_2S ~~in relation with~~related to hydrocarbons (e.g., Hill, 1987), or

Comentado [M41]: Reviewer #2
l615: for the sake of consistency, drop s at the end of CCG here.

Comentado [M42]: l636: (T) related to hydrocarbons

iii) the oxidation of sulfides (e.g., pyrite) disseminated in ~~limestones~~ carbonate rocks (e.g., Bottrell, 1991). In the case of Devaux cave marine evaporite rocks (e.g., of the Upper Triassic Keuper facies) and hydrocarbons are absent in the catchment of the cave. The most plausible explanation for the presence of dissolved sulfate in Devaux´s water is the oxidation of pyrite present in the limestone (du Cailar and Dubois, 1953; Requirand, 2014).

~~Water in Devaux cave contains moderate concentrations of sulfate.~~ $\delta^{34}S$ values of gypsum (-11.9 to -15.8 ‰), pyrite (-12.7 ‰), and dissolved sulfate (-14.4 ‰ in dripwater and -28.5 to -27.3 ‰ in Brulle spring water) are within the range of biogenic pyrite and differ notably from values of marine evaporites (10-35 ‰) (Seal, 2006). Thus, the $\delta^{34}S$ values together with the geological setting of the cave support the hypothesis that disseminated pyrite in the host limestone is the main source of dissolved sulfate and subsequently of CCG. Only the dissolved sulfate $\delta^{34}S$ values of Brulle spring are considerably more negative (-28.5‰ and -27.3‰). This may be a consequence of microbially mediated redox processes in the karst that discriminate against ^{34}S (Zerkle et al., 2016; Temovski et al., 2018). Further studies on the microbiology of the cave may shed light on these mechanisms and how the local sulfur cycle may have changed in the recent past.

In gypsum caves, dissolved sulfate dominates over the bicarbonate, and the typical crystallization sequence during freezing of water with high TDS is gypsum → carbonate (commonly calcite) → celestine (Žák et al., 2018). In Devaux cave, however, bicarbonate dominates over sulfate, and our observations show that gypsum crystals partly nucleated on CCC_{coarse}. Accordingly, the crystallization sequence at Devaux cave is calcite → gypsum, taking place in a semi-closed system at low freezing rates.

The second aspect that makes the CCG in Devaux cave unique is the size and ~~well-developed~~euhedral ~~crystal~~ shapes of the crystals (Fig. 9 b), which differ notably from the much smaller sizes of gypsum crystals (20-200 μm) and gypsum powders (1-30 μm) found in gypsum caves in Russia and Ukraine (Žák et al., 2018 and references therein). Another characteristic of CCC and CCG

Comentado [M43]: l666-667: (T) is the size and well-developed shape of the crystals

occurrences in Devaux cave is the presence of milky ice surrounding them (Fig. 9a, e) which seems to be related to the freezing process during the formation cryogenic minerals in a subaqueous environment.

Finally, the presence of gypsum aggregates overgrowing ~~some~~ blocks (Fig. 9c) supports the hypothesis of subaqueous gypsum formation. On the other hand, the absence of gypsum ~~was never observed~~ grow~~ths~~ing~~ing~~ ~~from~~ on the ceiling or on the walls~~,~~ ~~thus allowing~~allows ~~it~~ to discard its formation from seepage water followed by precipitation due to evaporation in the cave (e.g., Gázquez et al., 2017, 2020). In essence, all observations indicate that gypsum precipitated in a semi-closed subaqueous environment and has been preserved from later dissolution by the exceptionally dry environment of this ice cave. Gypsum precipitating from freezing waters has been also documented in the Arctic and the Antarctica (Losiak et al., 2016; Wollenburg et al., 2018) and has been proposed as a mechanism~~s~~ for gypsum formation on Mars (Losiak et al., 2016).

Comentado [M44]: Reviewer #1

lines 676-679: I think that this info could be moved forward in the section.

6. Conclusions

The investigation of Devaux ice cave, based on cave monitoring, geomorphology, and geochemical analyses, provides exceptional insights into the origin of modern and past mountain permafrost and associated processes and deposits.

- Devaux cave consists of two parts characterised by different thermal regimes: 1) the near-entrance parts and the main gallery showing large temperature fluctuations and cave air temperatures seasonally exceeding 0ºC. These passages are influenced by ~~an~~ advective air flow and ~~the~~ heat released by the cave river. 2) The inner sector and isolated chambers are characterized by muted thermal oscillations and temperatures constantly below 0ºC. There, the cave air temperature is mainly controlled by heat conduction through the bedrock.

- Devaux cave is impacted by backflooding in late winter/early spring when the main outlets freeze, damming the water inside the cave forming a lake. The blocking of the outlets requires temperatures below 0ºC in the Gavarnie cirque,

764 while on the southern side of the Monte Perdido massif, temperatures above
765 0ºC allow water infiltration.
766
767 - The absence of dripwater in most parts of the cave together with the presence
768 of perennial/seasonal hoarfrost, and the location of massive ice bodies on the
769 ceiling and/or filling cupulas and galleries are indicative of frozen bedrock
770 surrounding the cave. Permafrost at Devaux cave is attributed to a combination
771 of rock undercooling by cave air ventilation and the local climate setting giving
772 rise to the development and/or preservation of permafrost inherited from past
773 colder periods. Currently, permafrost seems to be present above the cave
774 reaching a maximum thickness of ~200 m and a lateral extension of ~350 m
775 towards the southern face of the Monte Perdido massif.
776
777 - We report the first deposits of cryogenic gypsum in a limestone-hosted ice cave.
778 Most of the cryogenic minerals are still within the ice and surrounded by milky
779 ice ~~ice~~ rich in air inclusions. Gypsum precipitation occurred subaqueously as a
780 result of slow freezing, following CCC formation. $\delta^{34}S$ values show that the
781 sulfate originated from the oxidation of pyrite present in the limestone.
782
783 - Current climate conditions seem to be still favourable for the preservation of ice
784 within this cave. This situation contrasts to the large ice mass loss in other ice
785 caves elsewhere. The ice deposits in Devaux cave allow unique insights into
786 processes leading to the formation of cryogenic carbonates and sulfates, and
787 represents ~~an ideal~~a unique site to better understand the mountain permafrost
788 evolution in the Monte Perdido massif and the Pyrenees in general.

Comentado [M45]: Reviewer #2:
l718: (T) rich in air inclusions

Comentado [M46]: Reviewer #1
line 723: Please consider adding "ice mass" between the word large and loss to clarify the meaning of the sentence.

Comentado [M47]: Reviewer #2
l724: (T) in Devaux cave

789 **Competing interests**

790 No competing of interest

791 **Authors contribution**

792 MB conceived the project, planned fieldwork and the sampling strategy. AM
793 obtained funding for this work. MB and GC installed and maintained the sensors
794 and performed the fieldwork. GC contributed with cave monitoring data from 2011
795 to 2015. MB analysed monitoring, geomorphological, and geochemical data. FG
796 performed $\delta^{34}S$ analyses using the facilities provided by AVT. JILM created the

radiation map. MB designed the figures and wrote a first draft of the manuscript. ML and CS significantly contributed to the discussion of the data. ML and AM reviewed all versions of the manuscript. All authors reviewed the manuscript and contributed to the results, discussion, and final interpretation. All authors approved its submission.

Acknowledgements

We thank the directorates of the Parc National des Pyrénées (France) and the Ordesa y Monte Perdido National Park (Spain) for their permission to investigate Devaux cave. We want to especially thank Marc Galy for his cave survey which improves noticeably previously published surveys and for the historical photo of 1984. Also, we thank Météo France for providing climate data from the Pic du midi de Bigorre station. We thank Maria Leunda for a critical review and suggestions to the first draft of the manuscript. We also thank Jerome Labat (SSPPO), Claude Novoa, Alvaro Palacios, Maria Leunda, José Leunda, David Serrano, the Góriz hut staff (www.goriz.es), and the Palazio family (www.hotelpalazio.com) for their invaluable help during fieldwork. We thank Paul Cluzon for the photo of Fig. 1d, and Claude Requirand for his report about Devaux cave. The authors would like to acknowledge the use of the Servicio General de Apoyo a la Investigación-SAI, University of Zaragoza, and Alberto Barcos (IPE-CSIC) for the chemical water analyses. This study contributes to the work carried out by the DGA research group Procesos Geoambientales y Cambio Global (ref.: E02-20R) and the MERS research group 2017 SGR 1588.

Financial support

This research has been supported by the following projects which were funded by the National Parks Autonomous Agency (OAPN) (OCHESTRA-ref 2552/2020), the Spanish Agencia Estatal de Investigación (AEI-Spain) (PICACHU-ref PID2019-106050RB-I00), (SPYRIT- ref CGL2016-77479-R), the PaleoICE EXPLORA project (ref. CGL2015-72167-EXP) and the Comité régional de spéléologie de Nouvelle Aquitaine. Miguel Bartolomé was supported by a postdoctoral fellowship of the Juan de la Cierva-Formación program provided by the Spanish Ministry of Science (ref.: FJCI-2017-31725) and OCHESTRA-ref 2552/2020. Fernando Gázquez was financially supported by a Ramón y Cajal

Fellowship (RYC2020-029811-I) of the Spanish Government (Ministerio de Economía y Competividad).

References

Badino, G., 2010. UNDERGROUND METEOROLOGY-"What's the weather underground?" Acta Carsologica 39. https://doi.org/10.3986/ac.v39i3.74

Bartolomé, M., Sancho, C., Benito, G., Medialdea, A., Calle, M., Moreno, A., Leunda, M., Luetscher, M., Muñoz, A., Bastida, J., Cheng, H., Edwards, R.L., 2021. Effects of glaciation on karst hydrology and sedimentology during the Last Glacial Cycle: The case of Granito cave, Central Pyrenees (Spain). CATENA 206, 105252. https://doi.org/10.1016/j.catena.2021.105252

Bartolomé, M., Sancho, C., Osácar, M.C., Moreno, A., Leunda, M., Spötl, C., Luetscher, M., López-Martínez, J., Belmonte, A., 2015. Characteristics of cryogenic carbonates in a Pyrenean ice cave (northern Spain). Geogaceta 58 107–110.

Belmonte-Ribas, Á., Sancho, C., Moreno, A., Lopez-Martinez, J., Bartolome, M., 2014. Present-day environmental dynamics in ice cave a294, central pyrenees, spain. Geogr. Fis. E Din. Quat. 37, 131–140. https://doi.org/10.4461/GFDQ.2014.37.12

Biskaborn, B.K., Smith, S.L., Noetzli, J., Matthes, H., Vieira, G., Streletskiy, D.A., Schoeneich, P., Romanovsky, V.E., Lewkowicz, A.G., Abramov, A., Allard, M., Boike, J., Cable, W.L., Christiansen, H.H., Delaloye, R., Diekmann, B., Drozdov, D., Etzelmüller, B., Grosse, G., Guglielmin, M., Ingeman-Nielsen, T., Isaksen, K., Ishikawa, M., Johansson, M., Johannsson, H., Joo, A., Kaverin, D., Kholodov, A., Konstantinov, P., Kröger, T., Lambiel, C., Lanckman, J.-P., Luo, D., Malkova, G., Meiklejohn, I., Moskalenko, N., Oliva, M., Phillips, M., Ramos, M., Sannel, A.B.K., Sergeev, D., Seybold, C., Skryabin, P., Vasiliev, A., Wu, Q., Yoshikawa, K., Zheleznyak, M., Lantuit, H., 2019. Permafrost is warming at a global scale. Nat. Commun. 10, 264. https://doi.org/10.1038/s41467-018-08240-4

Boeckli, L., Brenning, A., Gruber, S., Noetzli, J., 2012. A statistical approach to modelling permafrost distribution in the European Alps or similar mountain ranges. The Cryosphere 6, 125–140. https://doi.org/10.5194/tc-6-125-2012

Bottrell, S.H., 1991. Sulphur isotope evidence for the origin of cave evaporites in Ogof y Daren Cilau, south Wales. Mineral. Mag. 55, 209–210. https://doi.org/10.1180/minmag.1991.055.379.09

Bücher, A., Dessens, J., 1991. Secular Trend of Surface Temperature at an Elevated Observatory in the Pyrenees. J. Clim. 4, 859–868. https://doi.org/10.1175/1520-0442(1991)004<0859:STOSTA>2.0.CO;2

Casteret, N., 1953. Dans les glaces souterraines. Les plus éleveés de Monde. Libraire Académique Perrin, Paris, p. 93.

Colucci, R., Luetscher, M., Forteet, E., Guglielmin, M., Lenaz, D., Princivalle, F., Vita, F., 2017. First alpine evidence of in situ coarse cryogenic cave carbonates (CCCcoarse). Geogr. Fis. E Din. Quat. 53–59. https://doi.org/10.4461/GFDQ.2017.40.5

Colucci, R.R., Guglielmin, M., 2019. Climate change and rapid ice melt: Suggestions from abrupt permafrost degradation and ice melting in an alpine ice cave. Prog. Phys. Geogr. Earth Environ. 0309133319846056. https://doi.org/10.1177/0309133319846056

Dessens, J., Bücher, A., 1995. Changes in minimum and maximum temperatures at the Pic du Midi in relation with humidity and cloudiness, 1882–1984. Atmospheric Res., ~~Minimax Workshop~~ 37, 147–162. https://doi.org/10.1016/0169-8095(94)00075-O

Devaux, J., 1929. Nouvelle grotte Marboréenne. La Natura 102–107.

Devaux, J., 1933. La grotte des sœurs de la cascade. Études glaciologiques, 1920-1930. Tome VII, pp. 233-238. Plan & coupe. Paris. Imprimerie Nationale. Ministère de l'Agriculture. Direction des eaux et du génie rural.

du Cailar, J., Couderc, J., Dubois, P., 1953. La source du Gave de Pau. Annales de Spéléologie 181–203.

du Cailar, J., Dubois, P., 1953. Sur quelques modalités de formation et d´évolution des dépôts cristallins dans les cavités de haute altitude. In: Premier congrès international de spéléologie. Paris, Tome II, pp 325-333.

Dublyansky, Y., Moseley, G.E., Lyakhnitsky, Y., Cheng, H., Edwards, L.R., Scholz, D., Koltai, G., Spötl, C., 2018. Late Palaeolithic cave art and permafrost in the Southern Ural. Sci. Rep. 8, 12080. https://doi.org/10.1038/s41598-018-30049-w

Fankhauser, A., McDermott, F., Fleitmann, D., 2016. Episodic speleothem deposition tracks the terrestrial impact of millennial-scale last glacial climate variability in SW Ireland. Quat. Sci. Rev. 152, 104–117. https://doi.org/10.1016/j.quascirev.2016.09.019

Feuillet, T., 2011. Statistical Analyses of Active Patterned Ground Occurrence in the Taillon Massif (Pyrénées, France/Spain). Permafr. Periglac. Process. 22, 228–238. https://doi.org/10.1002/ppp.726

García-Ruiz, J.M., Palacios, D., Andrés, N. de, Valero-Garcés, B.L., López-Moreno, J.I., Sanjuán, Y., 2014. Holocene and 'Little Ice Age' glacial activity in the Marboré Cirque, Monte Perdido Massif, Central Spanish Pyrenees. The Holocene 24, 1439–1452. https://doi.org/10.1177/0959683614544053

García-Ruiz, J.M., Palacios, D., Andrés, N., López-Moreno, J.I., 2020. Neoglaciation in the Spanish Pyrenees: a multiproxy challenge. Mediterr. Geosci. Rev. 2, 21–36. https://doi.org/10.1007/s42990-020-00022-9

Gázquez, F., Bauska, T.K., Comas-Bru, L., Ghaleb, B., Calaforra, J.-M., Hodell, D.A., 2020. The potential of gypsum speleothems for paleoclimatology: application to the Iberian Roman Humid Period. Sci. Rep. 10, 14705. https://doi.org/10.1038/s41598-020-71679-3

Gázquez, F., Calaforra, J.M., Evans, N.P., Hodell, D.A., 2017. Using stable isotopes (δ17O, δ18O and δD) of gypsum hydration water to ascertain the role of water condensation in the formation of subaerial gypsum speleothems. Chem. Geol. 452, 34–46. https://doi.org/10.1016/j.chemgeo.2017.01.021

Gellatly, A.F., Grove, J.M., Switsur, V.R., 1992. Mid-Holocene glacial activity in the Pyrenees. The Holocene 2, 266–270. https://doi.org/10.1177/095968369200200309

Giesemann, A., Jaeger, H.-J., Norman, A.L., Krouse, H.R., Brand, W.A., 1994. Online Sulfur-Isotope Determination Using an Elemental Analyzer Coupled to a Mass Spectrometer. Anal. Chem. 66, 2816–2819. https://doi.org/10.1021/ac00090a005

Gomez Lende, M., Berenguer, F., Serrano, E., 2014. Morphology, ice types and thermal regime in a high mountain ice cave. First studies applying terrestrial laser scanner in the Ppeña Ceastil ice cave (Picos de Europa, Northern Spain). Geogr. Fis. E Din. Quat. 37, 141–150. https://doi.org/10.4461/GFDQ.2014.37.13

Gómez Lende, M., Serrano, E., Bordehore, L.J., Sandoval, S., 2016. The role of GPR techniques in determining ice cave properties: Peña Castil ice cave, Picos de Europa. Earth Surf. Process. Landf. 41, 2177–2190. https://doi.org/10.1002/esp.3976

Gómez-Ortiz, A., Oliva, M., Salvador-Franch, F., Palacios, D., Tanarro, L.M., de Sanjosé-Blasco, J.J., Salvà-Catarineu, M., 2019. Monitoring permafrost and periglacial processes in Sierra Nevada (Spain) from 2001 to 2016. Permafr. Periglac. Process. 30, 278–291. https://doi.org/10.1002/ppp.2002

Con formato: Alemán (Austria)

González Trueba, J.J., Moreno, R.M., Martínez de Pisón, E., Serrano, E., 2008. `Little Ice Age' glaciation and current glaciers in the Iberian Peninsula. The Holocene 18, 551–568. https://doi.org/10.1177/0959683608089209
Gruber, S., Haeberli, W., 2009. Mountain Permafrost, in: Margesin, R. (Ed.), Permafrost Soils, Soil Biology. Springer, Berlin, Heidelberg, pp. 33–44. https://doi.org/10.1007/978-3-540-69371-0_3
Gubler, S., Fiddes, J., Keller, M., Gruber, S., 2011. Scale-dependent measurement and analysis of ground surface temperature variability in alpine terrain. The Cryosphere 5, 431–443. https://doi.org/10.5194/tc-5-431-2011
Haeberli, W., Rellstab, W., Harrison, W.D., 1984. Geothermal Effects of 18 ka BP Ice Conditions in the Swiss Plateau. Ann. Glaciol. 5, 56–60. https://doi.org/10.3189/1984AoG5-1-56-60
Harris, C., Vonder Mühll, D., Isaksen, K., Haeberli, W., Sollid, J.L., King, L., Holmlund, P., Dramis, F., Guglielmin, M., Palacios, D., 2003. Warming permafrost in European mountains. Glob. Planet. Change 39, 215–225. https://doi.org/10.1016/j.gloplacha.2003.04.001
Heeb, B., 2014. The Next Generation of the DistoX Cave Surveying Instrument. CREG J., 88, 5-8.
Hercman, H., Gąsiorowski, M., Gradziński, M., Kicińska, D., 2010. The First Dating of Cave Ice from the Tatra Mountains, Poland and its Implication to Palaeoclimate Reconstructions. Geochronometria 36, 31–38. https://doi.org/10.2478/v10003-010-0016-2
Hill, C.A., 1987. Geology of Carlsbad Cavern and other caves in the Guadalupe Mountains, New Mexico and Texas. Bull 117 N. M. Bur. Mines Miner. Resour.
Hock, R., Rasul, G., Adler, C., Cáceres, B., Gruber, S., Hirabayashi, Y., Jackson, J., Kääb, A., Kang, S., Kutuzov, S., Milner, A., Molau, U., Morin, S., Orlove, B., Steltzer, H., 2019. High Mountain Areas. In: IPCC Special Report on the Ocean and Cryosphere in a Changing Climate.
Kern, Z., Bočić, N., Sipos, G., 2018. Radiocarbon-Dated Vegetal Remains from the Cave Ice Deposits of Velebit Mountain, Croatia. Radiocarbon 60, 1391–1402. https://doi.org/10.1017/RDC.2018.108
Kern, Z., Perşoiu, A., 2013. Cave ice – the imminent loss of untapped mid-latitude cryospheric palaeoenvironmental archives. Quat. Sci. Rev. 67, 1–7. https://doi.org/10.1016/j.quascirev.2013.01.008
Koltai, G., Spötl, C., Cheng, H., 2020. Cryogenic cave carbonates in the Dolomites (Northern Italy): insights into Younger Dryas cooling and seasonal precipitation. Clim. Past Discuss. 1–25. https://doi.org/10.5194/cp-2020-107
Korshunov, V.V., Shavrina, E.V., 1998. Gypsum speleothems of freezing origin. J. Cave Karst Stud. 60, 146–150.
Lechleitner, F.A., Mason, A.J., Breitenbach, S.F.M., Vaks, A., Haghipour, N., Henderson, G.M., 2020. Permafrost-related hiatuses in stalagmites: Evaluating the potential for reconstruction of carbon cycle dynamics. Quat. Geochronol. 56, 101037. https://doi.org/10.1016/j.quageo.2019.101037
Leunda, M., González-Sampériz, P., Gil-Romera, G., Bartolomé, M., Belmonte-Ribas, Á., Gómez-García, D., Kaltenrieder, P., Rubiales, J.M., Schwörer, C., Tinner, W., Morales-Molino, C., Sancho, C., 2019. Ice cave reveals environmental forcing of long-term Pyrenean tree line dynamics. J. Ecol. 107, 814–828. https://doi.org/10.1111/1365-2745.13077
Lewkowicz, A.G., Ednie, M., 2004. Probability mapping of mountain permafrost using the BTS method, Wolf Creek, Yukon Territory, Canada. Permafr. Periglac. Process. 15, 67–80. https://doi.org/10.1002/ppp.480
Li, T.-Y., Baker, J.L., Wang, T., Zhang, J., Wu, Y., Li, H.-C., Blyakharchuk, T., Yu, T.-L., Shen, C.-C., Cheng, H., Kong, X.-G., Xie, W.-L., Edwards, R.L., 2021. Early Holocene permafrost retreat in West Siberia amplified by reorganization of westerly wind systems. Commun. Earth Environ. 2, 1–11. https://doi.org/10.1038/s43247-021-00238-z

López-Moreno, J.I., Alonso-González, E., Monserrat, O., Del Río, L.M., Otero, J., Lapazaran, J., Luzi, G., Dematteis, N., Serreta, A., Rico, I., Serrano-Cañadas, E., Bartolomé, M., Moreno, A., Buisan, S., Revuelto, J., 2019. Ground-based remote-sensing techniques for diagnosis of the current state and recent evolution of the Monte Perdido Glacier, Spanish Pyrenees. J. Glaciol. 65, 85–100. https://doi.org/10.1017/jog.2018.96

López-Moreno, J.I., Revuelto, J., Rico, I., Chueca-Cía, J., Julián, A., Serreta, A., Serrano, E., Vicente-Serrano, S.M., Azorin-Molina, C., Alonso-González, E., García-Ruiz, J.M., 2016. Thinning of the Monte Perdido Glacier in the Spanish Pyrenees since 1981. The Cryosphere 10, 681–694. https://doi.org/10.5194/tc-10-681-2016

Losiak, A., Derkowski, A., Skała, A., Trzciński, J., 2016. Evaporites on ice: how to form gypsum on Antartica and on Martian North polar residual cap? In: 47th Lunar and Planetary Science Conference. 1972.pdf.

Luetscher, M., Bolius, D., Schwikowski, M., Schotterer, U., Smart, P.L., 2007. Comparison of techniques for dating of subsurface ice from Monlesi ice cave, Switzerland. J. Glaciol. 53, 374–384.

Luetscher, M., Borreguero, M., Moseley, G.E., Spötl, C., Edwards, R.L., 2013. Alpine permafrost thawing during the Medieval Warm Period identified from cryogenic cave carbonates. The Cryosphere 7, 1073–1081. https://doi.org/10.5194/tc-7-1073-2013

Luetscher, M., Jeannin, P.-Y., 2018. Chapter 12 - Ice Caves in Switzerland, in: Perşoiu, A., Lauritzen, S.-E. (Eds.), Ice Caves. Elsevier, pp. 221–235. https://doi.org/10.1016/B978-0-12-811739-2.00010-3

Luetscher, M., Lismonde, B., Jeannin, P.-Y., 2008. Heat exchanges in the heterothermic zone of a karst system: Monlesi cave, Swiss Jura Mountains. J. Geophys. Res. Earth Surf. 113. https://doi.org/10.1029/2007JF000892

Lundberg, J., McFarlane, D.A., 2007. Pleistocene depositional history in a periglacial terrane: A 500 k.y. record from Kents Cavern, Devon, United Kingdom. Geosphere 3, 199–219. https://doi.org/10.1130/GES00085.1

Marshall, P., Brown, M.C., 1974. Ice in Coulthard Cave, Alberta. Can. J. Earth Sci. https://doi.org/10.1139/e74-045

Mavlyudov, B.R., 2008. Caves Glaciation in the Past. Федеральное государственное бюджетное учреждение науки Институт географии Российской академии наук, pp. 499–505.

Moseley, G.E., Edwards, R.L., Lord, N.S., Spötl, C., Cheng, H., 2021. Speleothem record of mild and wet mid-Pleistocene climate in northeast Greenland. Sci. Adv. 7, eabe1260. https://doi.org/10.1126/sciadv.abe1260

Munroe, J., Kimble, K., Spötl, C., Marks, G.S., McGee, D., Herron, D., 2021. Cryogenic cave carbonate and implications for thawing permafrost at Winter Wonderland Cave, Utah, USA. Sci. Rep. 11, 6430. https://doi.org/10.1038/s41598-021-85658-9

Munroe, J.S., 2021. First investigation of perennial ice in Winter Wonderland Cave, Uinta Mountains, Utah, USA. The Cryosphere 15, 863–881. https://doi.org/10.5194/tc-15-863-2021

Navarro-Serrano, F., López-Moreno, J.I., Azorin-Molina, C., Alonso-González, E., Tomás-Burguera, M., Sanmiguel-Vallelado, A., Revuelto, J., Vicente-Serrano, S.M., 2018. Estimation of near-surface air temperature lapse rates over continental Spain and its mountain areas. Int. J. Climatol. 38, 3233–3249. https://doi.org/10.1002/joc.5497

Noetzli, J., Gruber, S., 2009. Transient thermal effects in Alpine permafrost. The Cryosphere 3, 85–99. https://doi.org/10.5194/tc-3-85-2009

Orvošová, M., Deininger, M., Milovský, R., 2014. Permafrost occurrence during the Last Permafrost Maximum in the Western Carpathian Mountains of Slovakia as inferred from cryogenic cave carbonate. Boreas 43, 750–758. https://doi.org/10.1111/bor.12042

Perşoiu, A., Buzjak, N., Onaca, A., Pennos, C., Sotiriadis, Y., Ionita, M., Zachariadis, S., Styllas, M., Kosutnik, J., Hegyi, A., Butorac, V., 2021. Record summer rains in 2019 led to massive loss of surface and cave ice in SE Europe. The Cryosphere 15, 2383–2399. https://doi.org/10.5194/tc-15-2383-2021

Perşoiu, A., Lauritzen, S.-E. (Eds.), 2018. Ice caves. Elsevier, Amsterdam, Netherlands.

Perşoiu, A., Onac, B.P., Wynn, J.G., Blaauw, M., Ionita, M., Hansson, M., 2017. Holocene winter climate variability in Central and Eastern Europe. Sci. Rep. 7, 1196. https://doi.org/10.1038/s41598-017-01397-w

Pons, X., Ninyerola, M., 2008. Mapping a topographic global solar radiation model implemented in a GIS and refined with ground data. Int. J. Climatol. 28, 1821–1834. https://doi.org/10.1002/joc.1676

Racine, T.M.F., Spötl, C., Reimer, P.J., Čarga, J., 2022. RADIOCARBON CONSTRAINTS ON PERIODS OF POSITIVE CAVE ICE MASS BALANCE DURING THE LAST MILLENNIUM, JULIAN ALPS (NW SLOVENIA). Radiocarbon 1–24. https://doi.org/10.1017/RDC.2022.26

Reille, M., Andrieu, V., 1995. The late Pleistocene and Holocene in the Lourdes Basin, Western Pyrénées, France: new pollen analytical and chronological data. Veg. Hist. Archaeobotany 4, 1–21. https://doi.org/10.1007/BF00198611

Requirand, C., 2014. Hypothèse sur la formation des cristaux de gypse Grotte Glacée Devaux (Gavarnie - Hautes Pyrénées). Bulletin de la Société Ramon. 11 pp.

Richter, D.K., Meissner, P., Immenhauser, A., Schulte, U., Dorsten, I., 2010a. Cryogenic and non-cryogenic pool calcites indicating permafrost and non-permafrost periods: a case study from the Herbstlabyrinth-Advent Cave system (Germany). The Cryosphere 4, 501–509. https://doi.org/10.5194/tc-4-501-2010

Richter, D.K., Meissner, P., Immenhauser, A., Schulte, U., Dorsten, I., 2010b. Cryogenic and non-cryogenic pool calcites indicating permafrost and non-permafrost periods: a case study from the Herbstlabyrinth-Advent Cave system (Germany). The Cryosphere 4, 501–509. https://doi.org/10.5194/tc-4-501-2010

Rico, I., Magnin, F., López Moreno, J.I., Serrano, E., Alonso-González, E., Revuelto, J., Hughes-Allen, L., Gómez-Lende, M., 2021. First evidence of rock wall permafrost in the Pyrenees (Vignemale peak, 3,298 m a.s.l., 42°46’16”N/0°08’33”W). Permafr. Periglac. Process. 32, 673–680. https://doi.org/10.1002/ppp.2130

Rodríguez-Salgado, P., Oms, O., Ibáñez-Insa, J., Anadón, P., Gómez de Soler, B., Campeny, G., Agustí, J., 2021. Mineralogical proxies of a Pliocene maar lake recording changes in precipitation at the Camp dels Ninots (Pliocene, NE Iberia). Sediment. Geol. 418, 105910. https://doi.org/10.1016/j.sedgeo.2021.105910

Rösch, G., Rösch, J., 1935. Visites à la grotte Devaux. La Montagne. Revue du Club Alpin Français, N° 269, pp.171-178.

Rösch, J., 1949. Une exploration de la Grotte Devaux à Gavarnie. Bulletin de la section du Sud-Ouest de la Club Alpin Français, N°69. pp. 103-107.

Sancho, C., Arenas, C., Pardo, G., Peña-Monné, J.L., Rhodes, E.J., Bartolomé, M., García-Ruiz, J.M., Martí-Bono, C., 2018a. Glaciolacustrine deposits formed in an ice-dammed tributary valley in the south-central Pyrenees: New evidence for late Pleistocene climate. Sediment. Geol. 366, 47–66. https://doi.org/10.1016/j.sedgeo.2018.01.008

Sancho, C., Belmonte, Á., Bartolomé, M., Moreno, A., Leunda, M., López-Martínez, J., 2018b. Middle-to-late Holocene palaeoenvironmental reconstruction from the A294 ice-cave record (Central Pyrenees, northern Spain). Earth Planet. Sci. Lett. 484, 135–144. https://doi.org/10.1016/j.epsl.2017.12.027

Sancho, C., Peña, J.L., Mikkan, R., Osácar, C., Quinif, Y., 2004. Morphological and speleothemic development in Brujas Cave (Southern Andean Range, Argentine): palaeoenvironmental significance. Geomorphology 57, 367–384. https://doi.org/10.1016/S0169-555X(03)00166-1

Scandroglio, R., Draebing, D., Offer, M., Krautblatter, M., 2021. 4D quantification of alpine permafrost degradation in steep rock walls using a laboratory-calibrated electrical resistivity tomography approach. Surf. Geophys. 19, 241–260. https://doi.org/10.1002/nsg.12149

Seal, R.R., II, 2006. Sulfur Isotope Geochemistry of Sulfide Minerals. Rev. Mineral. Geochem. 61, 633–677. https://doi.org/10.2138/rmg.2006.61.12

Serrano, E., Gómez-Lende, M., Belmonte, Á., Sancho, C., Sánchez-Benítez, J., Bartolomé, M., Leunda, M., Moreno, A., Hivert, B., 2018. Chapter 28 - Ice Caves in Spain, in: Perşoiu, A., Lauritzen, S.-E. (Eds.), Ice Caves. Elsevier, pp. 625–655. https://doi.org/10.1016/B978-0-12-811739-2.00028-0

Serrano, E., López-Moreno, J.I., Gómez-Lende, M., Pisabarro, A., Martín-Moreno, R., Rico, I., Alonso-González, E., 2020. Frozen ground and periglacial processes relationship in temperate high mountains: a case study at Monte Perdido-Tucarroya area (The Pyrenees, Spain). J. Mt. Sci. 17, 1013–1031. https://doi.org/10.1007/s11629-019-5614-5

Serrano, E., Sanjosé-Blasco, J.J. de, Gómez-Lende, M., López-Moreno, J.I., Pisabarro, A., Martínez-Fernández, A., 2019. Periglacial environments and frozen ground in the central Pyrenean high mountain area: Ground thermal regime and distribution of landforms and processes. Permafr. Periglac. Process. 30, 292–309. https://doi.org/10.1002/ppp.2032

Spötl, C., Cheng, H., 2014. Holocene climate change, permafrost and cryogenic carbonate formation: insights from a recently deglaciated, high-elevation cave in the Austrian Alps. Clim. Past 10, 1349–1362. https://doi.org/10.5194/cp-10-1349-2014

Spötl, C., Koltai, G., Jarosch, A.H., Cheng, H., 2021. Increased autumn and winter precipitation during the Last Glacial Maximum in the European Alps. Nat. Commun. 12, 1839. https://doi.org/10.1038/s41467-021-22090-7

Spötl, C., Reimer, P.J., Luetscher, M., 2011. Long-term mass balance of perennial firn and ice in an Alpine cave (Austria): Constraints from radiocarbon-dated wood fragments. The Holocene 0959683613515729. https://doi.org/10.1177/0959683613515729

Stoffel, M., Luetscher, M., Bollschweiler, M., Schlatter, F., 2009. Evidence of NAO control on subsurface ice accumulation in a 1200 yr old cave-ice sequence, St. Livres ice cave, Switzerland. Quat. Res. 72, 16–26. https://doi.org/10.1016/j.yqres.2009.03.002

Supper, R., Ottowitz, D., Jochum, B., Römer, A., Pfeiler, S., Kauer, S., Keuschnig, M., Ita, A., 2014. Geoelectrical monitoring of frozen ground and permafrost in alpine areas: field studies and considerations towards an improved measuring technology. Surf. Geophys. 12, 93–115. https://doi.org/10.3997/1873-0604.2013057

Temovski, M., Futó, I., Túri, M., Palcsu, L., 2018. Sulfur and oxygen isotopes in the gypsum deposits of the Provalata sulfuric acid cave (Macedonia). Geomorphology 315, 80–90. https://doi.org/10.1016/j.geomorph.2018.05.010

Vaks, A., Gutareva, O.S., Breitenbach, S.F.M., Avirmed, E., Mason, A.J., Thomas, A.L., Osinzev, A.V., Kononov, A.M., Henderson, G.M., 2013. Speleothems Reveal 500,000-Year History of Siberian Permafrost. Science 340, 183–186. https://doi.org/10.1126/science.1228729

Vaks, A., Mason, A.J., Breitenbach, S.F.M., Kononov, A.M., Osinzev, A.V., Rosensaft, M., Borshevsky, A., Gutareva, O.S., Henderson, G.M., 2020. Palaeoclimate evidence of vulnerable permafrost during times of low sea ice. Nature 577, 221–225. https://doi.org/10.1038/s41586-019-1880-1

Wind, M., Obleitner, F., Racine, T., Spötl, C., 2022. Multi-annual temperature evolution and implications for cave ice development in a sag-type ice cave in the Austrian Alps. Cryosphere Discuss. 1–26. https://doi.org/10.5194/tc-2022-67

Wollenburg, J.E., Katlein, C., Nehrke, G., Nöthig, E.-M., Matthiessen, J., Wolf- Gladrow, D.A., Nikolopoulos, A., Gázquez-Sanchez, F., Rossmann, L., Assmy, P., Babin, M., Bruyant, F.,

Beaulieu, M., Dybwad, C., Peeken, I., 2018. Ballasting by cryogenic gypsum enhances carbon export in a Phaeocystis under-ice bloom. Sci. Rep. 8, 7703. https://doi.org/10.1038/s41598-018-26016-0

Yonge, C.J., Ford, D., Horne, G., Lauriol, B., Schroeder, J., 2018. Chapter 15 - Ice Caves in Canada, in: Perşoiu, A., Lauritzen, S.-E. (Eds.), Ice Caves. Elsevier, pp. 285–334. https://doi.org/10.1016/B978-0-12-811739-2.00015-2

Žák, K., Onac, B.P., Kadebskaya, O.I., Filippi, M., Dublyansky, Y., Luetscher, M., 2018. Chapter 6 - Cryogenic Mineral Formation in Caves, in: Perşoiu, A., Lauritzen, S.-E. (Eds.), Ice Caves. Elsevier, pp. 123–162. https://doi.org/10.1016/B978-0-12-811739-2.00035-8

Žák, K., Richter, D.K., Filippi, M., Živor, R., Deininger, M., Mangini, A., Scholz, D., 2012. Coarsely crystalline cryogenic cave carbonate – a new archive to estimate the Last Glacial minimum permafrost depth in Central Europe. Clim. Past 8, 1821–1837. https://doi.org/10.5194/cp-8-1821-2012

Žák, K., Urban, J., Cílek, V., Hercman, H., 2004. Cryogenic cave calcite from several Central European caves: age, carbon and oxygen isotopes and a genetic model. Chem. Geol. 206, 119–136. https://doi.org/10.1016/j.chemgeo.2004.01.012

Zerkle, A.L., Jones, D.S., Farquhar, J., Macalady, J.L., 2016. Sulfur isotope values in the sulfidic Frasassi cave system, central Italy: A case study of a chemolithotrophic S-based ecosystem. Geochim. Cosmochim. Acta 173, 373–386. https://doi.org/10.1016/j.gca.2015.10.028

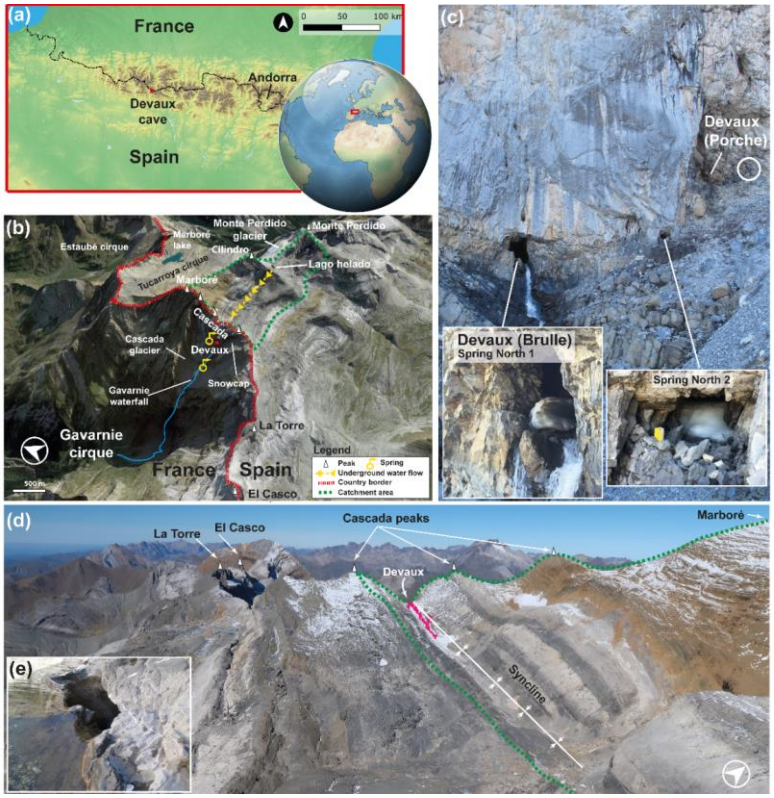

Figure 1. (a) Location of Devaux cave in the Central Pyrenees (ASTER GDEM, NASA v3, 2019). (b) Satellite image and location of Devaux cave, main peaks, lakes, glaciers and cirques in the study area (3D ©Google Earth). The yellow arrows indicate the underground flow path from Lago helado to the Gavarnie waterfall according to the dye-tracing experiment of du Cailar et al., (1953). (c) View towards the entrances of Devaux cave. The lower entrance (~2821 m a.s.l.) corresponds to the Brulle spring (Spring North 1), while the upper one corresponds to the main entrance (Porche (South), ~2836 m a.s.l.). Spring North 2 is located between both entrances. Note person for scale (within the white circle). Remnants of ice partially blocking Brulle and Spring North 2 (July 2021). (d) Landscape view of the catchment area and approximate location of Devaux cave (in dark pink; photo: Paul Cluzon). (e) Ponor located on the southern shore of Lago Helado.

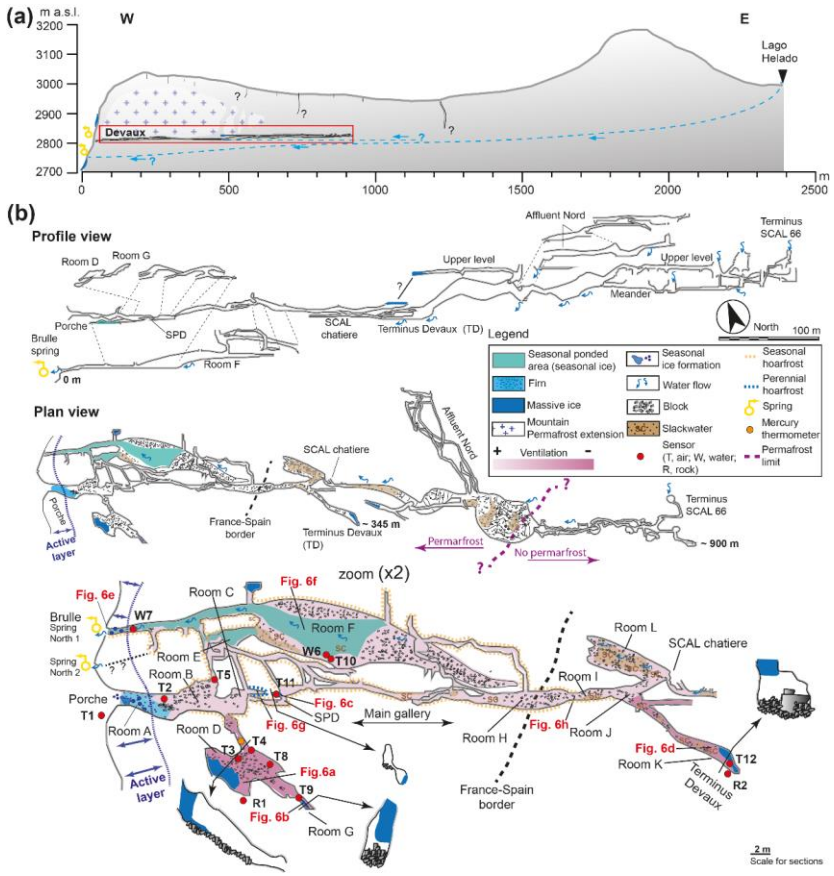

Figure 2. (a) Schematic W-E cross section from Lago helado to Devaux cave, the assumed extent of mountain permafrost, and ~~and~~ the interpreted underground flow path according to du Cailar et al., (1953). (b) Longitudinal section and plan view of Devaux cave showing the locations of sensors and cave deposits. Labels R, W and T refer to rock, water and air temperature sensors, respectively. The enlarged area corresponds to the first ~345 m of the studied sector. Red labels correspond to the approximate location of the photographs in Fig. ~~7~~6. Cave survey by Marc Galy, Groupe Spéléologique des Pyrénées (GSPY 86).

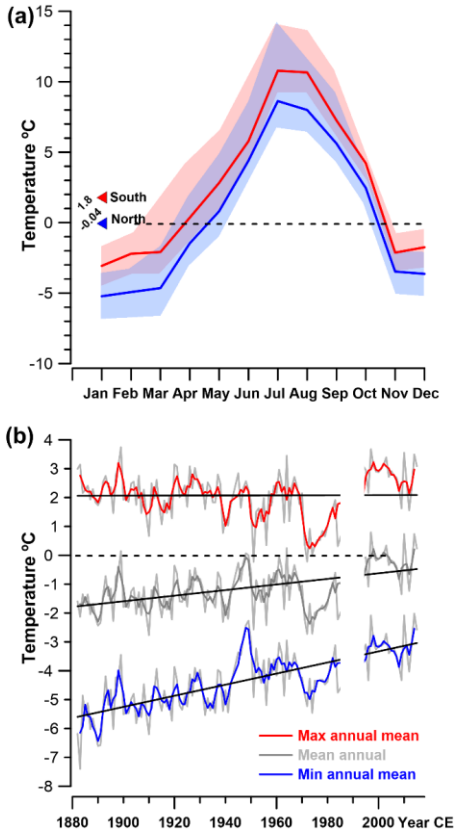

Figure 3. (a) Monthly temperature variation on the northern and southern side of the Monte Perdido massif. Red and blue triangles correspond to the 4-year means. The dashed black line indicates 0ºC. Light red and blue shaded envelopes represent the maximum and minimum mean monthly temperatures, respectively. (b) Maximum, mean and minimum annual temperatures recorded at the Pic du Midi de Bigorre station since 1882. Black line indicates the general trend and dashed black line corresponds to 0ºC.

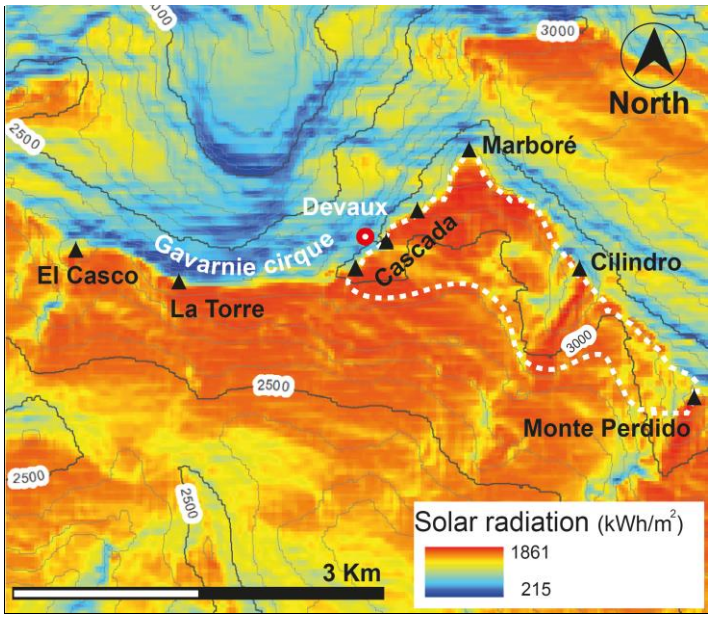

Figure 4. Solar radiation map of the study area. The solar radiation anomaly observed in the Gavarnie cirque is explained by its northerly orientation and the cirque morphology. Black triangles indicate the main peaks above 3000 m. The red-white circle marks Devaux cave, while the dashed white line delineates the approximate catchment.

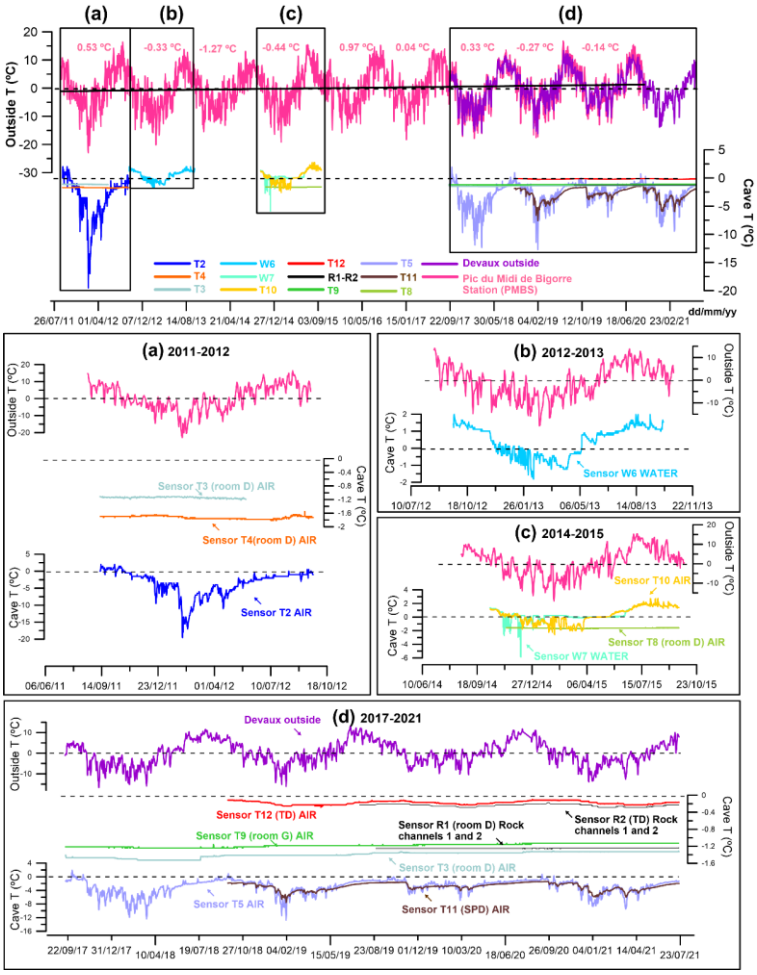

Figure 5. Mean daily air temperature variations at the Pic du Midi de Bigorre station (2860 m a.s.l., red), daily outside air temperature at Devaux cave (2836 m a.s.l., purple) and temperature variations in air, water and rock in the cave for the different time windows since 2011. Dark pink numbers are mean annual air temperatures (MAAT) at the Pic du Midi de Bigorre station (PMBS). Dashed lines indicate 0 ºC. Black squares labelled a, b, c, and d correspond to the areas enlarged below. The black continuous line is the external temperature trend during the monitoring period.

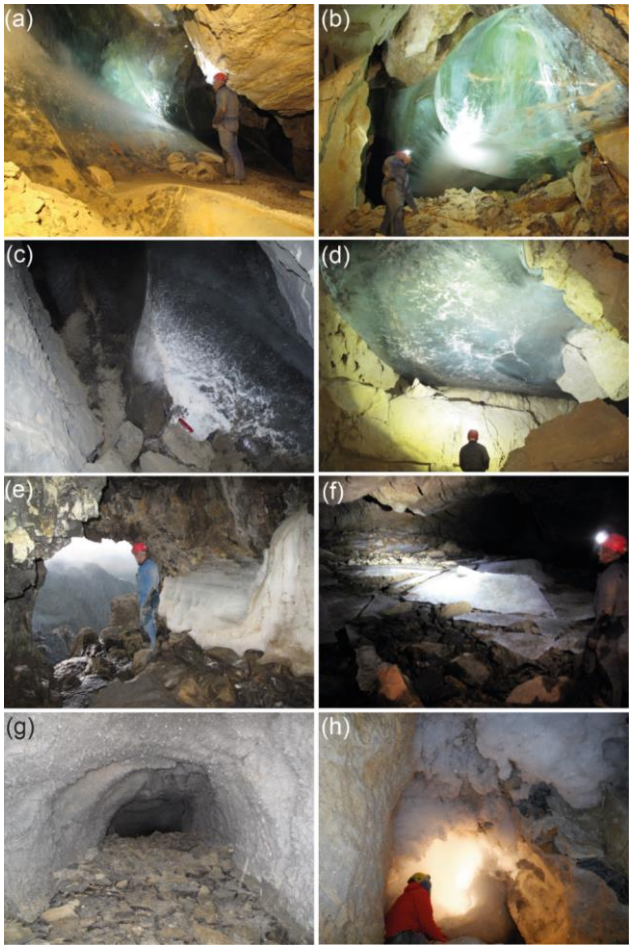

Figure 6. (a) Upper part of the ice body in room D. (b) Ice body hanging from the ceiling and the southwest wall in room G. White ~~colours~~ spots ~~at~~ near the bottom of the deposit correspond to ~~the concentration of~~ air inclusions as well as cryogenic carbonates and gypsum in the ice. (c) Small ice body in room SPD with CCC-CCG on and within the ice. Red knife (9 cm) for scale. (d) Ice body on the ceiling of room K (Terminus Devaux, TD). (e) Brulle spring and remains of a layered ice body (September 2018). (f) Broken ice sheets in the flooded area in room F (September 2018). (g) Millimetre to centimetre size perennial hoarfrost in a blind gallery below SPD room. (h) Seasonal hoarfrost aggregates (>30 cm long size) covering a cupola close to room J.

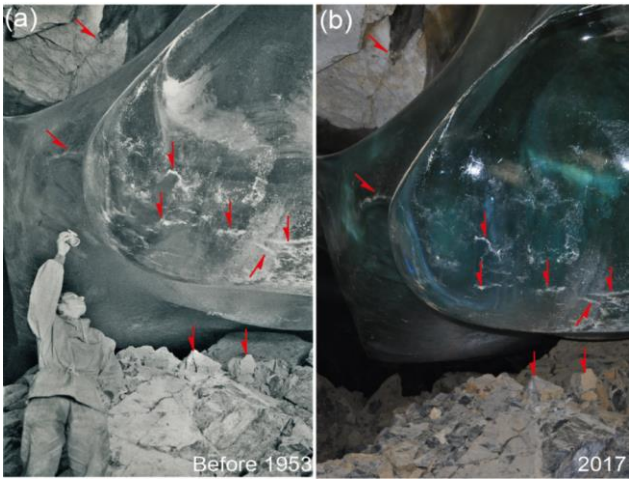

Figure 7. (a) Photo of the ice body located in room G taken shortly before 1953 (Casteret, 1953). (b) Photo taken in 2017. In both pictures, white patches on the ice surface correspond to small CCC accumulations released from the ice by sublimation. Red arrows indicate common features in both images.

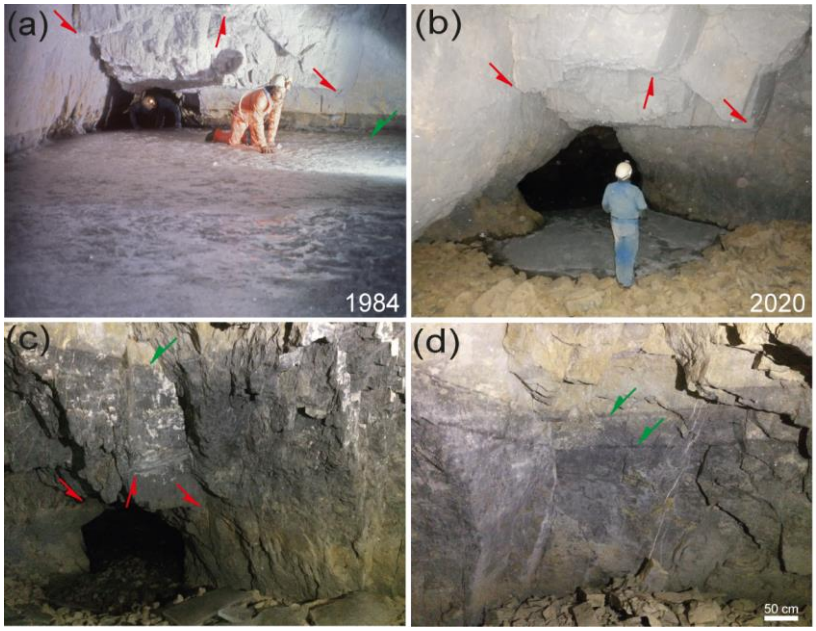

Figure 8. (a) Photo taken close to the river sector that connects the rooms F and E. The estimated ice level is 5 m higher than the Brulle spring. Photo by Jean Luc Bernardin (8th August 1984). (b) Similar area in 2020, and maximum extension of the seasonal lake ice formed during winter. (c) Higher ice mark level (c. +9.5 m with respect to the Brulle spring) and remnants of ice sheets from the frozen lake in 2018. (d) Two ice level marks (c. +9.2 m and +8.8 m with respect to the Brulle spring) located between the highest mark and the elevation of the ice in photo (a). In all images red arrows indicate the same rock edges, while green arrows show ice-level marks.

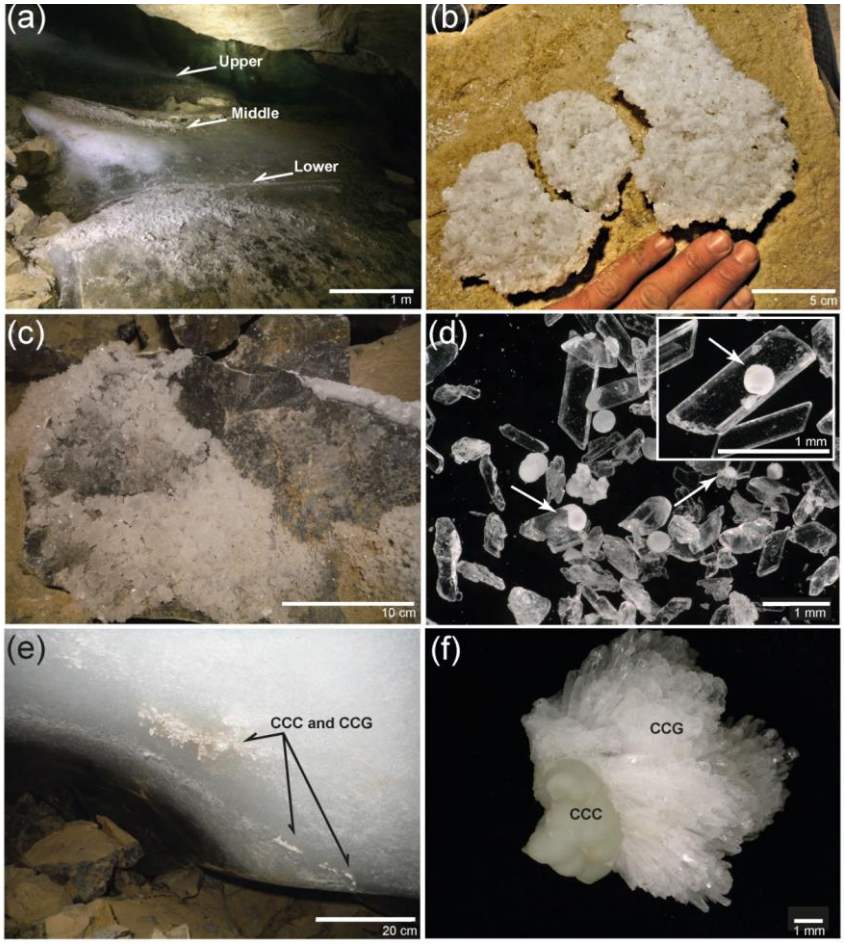

Figure 9. (a) Ice body in room G and three levels marked by cryogenic gypsum partially still in situ in the ice. The white~~st~~ area corresponds to milky ice with a high abundance of air inclusions. Gypsum crystals cover parts of the surface of the ice body due to ice retreat. (b) Large gypsum "raft" deposited on a block in room D. (c) Block in room D with gypsum overgrowths. (d) Microscopic image of euhedral CCG with ~~local~~ cores of CCC (white arrows), globular CCC, and ~~detail~~ enlarged image of euhedral gypsum crystal with a ~~core~~ nucleus of globular CCC. (e) CCC and CCG entrapped within milky ice in room G. (f) Detail of a CCC sample from room G covered by CCG.

		Cations					Anions								
Date	Sample	Na^+	NH_4^+	K^+	Ca^{2+}	Mg^{2+}	F^-	Cl^-	NO_2^-	Br^-	NO_3^-	SO_4^{2-}	HCO_3^-	CO_3^{2-}	PO_4^{3-}
15/09/2017	Devaux river 1	1.6	0.0	0.5	36.0	8.5	0.0	0.2	0.0	0.0	1.8	21.6	61.0	11.6	0.0
	Devaux drip 1	0.9	0.1	0.5	50.5	18.2	0.1	0.5	0.0	0.0	6.8	67.4	95.2	0.0	0.0
	Devaux drip 2	1.4	1.2	1.3	53.2	19.5	0.1	1.1	0.1	0.0	7.4	70.1	101.3	0.0	0.0
	Devaux Ice 1 (room D)	2.3	0.0	0.3	24.8	2.7	0.1	1.3	0.0	0.0	0.7	19.0	23.9	1.0	0.0
	Devaux Ice 2 (room D)	2.2	1.3	2.5	27.8	2.0	0.0	2.1	0.0	0.0	1.5	17.0	30.7	0.0	0.0
22/07/2018	Devaux river 1	0.6	0.0	0.4	32.4	4.4	0.0	0.2	0.0	0.0	0.9	5.1	53.7	4.0	0.1
	Devaux river 2	0.6	0.0	0.4	32.2	4.4	0.0	0.2	0.0	0.0	0.9	5.1	56.1	2.6	0.0
	Devaux drip 1	1.4	0.0	3.2	61.0	20.8	0.2	2.2	0.0	0.0	14.1	76.0	84.2	5.6	0.0
	Devaux drip 2	2.3	0.1	1.7	60.8	21.0	0.2	2.2	0.0	0.0	14.1	76.9	91.5	4.4	0.0
22/09/2018	Devaux river 1*	1.3	0.0	0.4	40.5	7.9	0.0	0.3	0.0	0.0	2.0	17.0	65.9	0.0	0.0
	Devaux drip 1*	1.6	0.0	1.2	70.6	27.2	0.2	1.1	0.0	0.0	19.8	116.5	90.3	0.0	0.0
28/07/2020	Devaux ice (seasonal)*	0.4	0.0	0.5	28.2	1.1	0.1	0.5	0.0	0.0	0.5	2.8	36.6	0.0	0.0
	Devaux river 1*	0.6	0.0	0.3	31.5	4.1	0.0	0.2	0.0	0.0	0.8	5.9	58.6	0.0	0.0
	Devaux drip 1*	1.1	0.2	1.1	42.3	12.5	0.1	0.5	0.0	0.0	2.9	38.4	101.3	0.0	0.0
	Devaux drip 2*	1.1	0.1	1.0	43.6	13.5	0.1	0.4	0.0	0.0	2.7	38.2	89.1	0.0	0.0
	Devaux drip 3*	1.6	0.7	1.5	47.9	13.1	0.1	1.1	0.0	0.0	2.2	36.7	107.4	0.0	0.0
26/07/2021	Devaux drip 1	2.9	0.0	1.1	83	35.9	0.3	5.9	0.6	0.1	40.2	269.3	104.9	0.0	0.0
	Devaux drip 2	3.3	0.4	2.0	73.2	29.3	0.2	6.0	0.1	0.0	28.6	212	112.2	0.0	0.0
	Devaux river 1	0.4	0.0	0.1	25.7	4.3	0.1	2.6	0.1	0.0	3.2	16.3	68.3	0.0	0.0
13/08/2021	Devaux river 1	0.7	0.0	0.2	28.6	4.9	0.1	2.6	0.0	0.0	1.5	20.4	74.4	0.0	0.0
	Devaux drip 1	7.5	2.2	5.1	49.5	15.2	0.2	10.3	0.3	0.0	6.9	77.3	130.5	0.0	0.0
	Devaux drip 2	5.1	1.3	2.8	49.3	15.6	0.2	6.5	0.1	0.0	6.5	80.5	129.3	0.0	0.0

Table 1. Chemical composition of water and ice samples from Devaux cave (in mg/l). * Samples where TDS (total dissolved solids) was calculated.

Location	Sample and description	$\delta^{34}S$ (‰) VCDT
Room D	Gypsum crystal (part of large raft)	-15.8
Room D	Gypsum crystal (part of large raft)	-15.5
Room D; lower gypsum level	Gypsum crystal (individual)	-15.6
Room D; middle gypsum level	Gypsum crystal (individual)	-15.0
Room D; middle gypsum level	Gypsum crystal (individual)	-15.6
Room D; upper gypsum level	Tiny gypsum crystals (aliquot)	-15.3
Room D	Gypsum crystal (individual)	-15.1
Room G	Gypsum crystal (individual)	-12.3
Room G	Gypsum overgrowth (individual)	-12.1
Room G	Gypsum overgrowth (individual)	-11.9
Room G	Gypsum overgrowth (individual)	-12.1
Room G	Gypsum overgrowth (individual)	-12.0
Limestone above cave	Pyrite crystal (individual)	-12.7
Entrance “Porche”	Drip water (1 liter)	-14.4
Brulle spring	River water 1 (1 liter)	-28.5
Brulle spring	River water 2 (1 liter)	-27.3

Table 2. Sulfur isotope values of gypsum, water and pyrite from Devaux.